CHAPTER 5 RECONSTRUCTION OF THE HISTORY OF HYDROTHERMAL ACTIVITY AND MINERAL FORMATION IN THE OCEANS BASED ON THE STUDIES OF METALLIFEROUS SEDIMENTS

While direct study of hydrothermal activity and the associated mineral formation as well as study of their scales are possible in the modern ocean, researchers are deprived of such opportunity for past geologic time. Even in cases where hydrothermal deposits that formed in the geological past are preserved they have been covered by sediments or overlain by lava and have become inaccessible after a time for observation and sampling. Rarely are these buried hydrothermal deposits found during deep-sea drilling or coring operations, and their direct study on an ocean scale is impossible at present. Even within hydrothermal fields, without special preliminary detailed surveys, the probability of intersecting hydrothermal edifices that are covered by sediments becomes a rare event. For example, within the TAG hydrothermal field, which has an area of about 25 km^2, after many years of investigations only once has a gravity core intersected a gossan over a sediment-covered hydrothermal mound (Bogdanov et al. 1995b). Studies of the metalliferous sediments sampled in the gravity- and piston cores, and in the cores obtained in the deep-sea drilling program can be very useful for the reconstruction of the history of hydrothermal activity and mineral formation.

Only a small part of the metal-bearing hydrothermal matter contributed to the ocean by high-temperature hydrothermal solutions accumulates in massive hydrothermal bodies. A prevalent part of this matter accumulates in the bottom sediments in the regions adjacent to the centers of hydrothermal activity. It has been shown in the previous chapters that, taking into account the distance from hydrothermal fields and/or vents and in the absence of the redeposition of sediment material, the accumulation rate of the hydrothermal metal-bearing matter in both proximal- and in distal metalliferous and low-metalliferous sediments reflects the intensity of the hydrothermal activity and, as a consequence, the amount of mineral formation

and deposition associated with it. As for the proximal metalliferous sediments, their composition also reflects metallogenic specialization of the hydrothermal fluids and the massive accumulation of sulfide minerals. The accumulation of coarse-grained proximal metalliferous sediment reflects stages of active hydrothermal discharge and the partial destruction of massive hydrothermal bodies. These properties of the metalliferous sediments enable their use in reconstructing the location and intensity of hydrothermal activity and mineral formation in past geological time, and in determining areas of present location of buried hydrothermal deposits.

5.1. Reconstruction of the history of hydrothermal activity and mineral formation based on the studies of sediment cores

The Active hydrothermal mound in the **TAG hydrothermal field** was the first massive hydrothermal accumulation where attempts have been made to reconstruct the history of hydrothermal activity and the mineral formation with use of data from studies of proximal metalliferous sediments (Lisitzin et al. 1989, 1990; Bogdanov et al. 1992). Core AMK-1785 (Fig. 5.1, 5.2) was chosen for this reconstruction.

Two layers that have high contents of Fe and Cu, the main hydrothermal metals in the metalliferous sediments from the TAG hydrothermal field Sect. 1.6.1), are noticeable in the core. Mineral indicators of the greenstone alteration of the basalt rocks are present in the sediments. Their total content in the carbonate-free part of the sandy-silt grain size fraction of the sediments rarely exceeds 5%. But increased contents exceeding 10% exist in two horizons at 145–147 cm and 32–35 cm in the core. Their ages as dated are 24–25 ka and 15–17 ka and are located immediately below the layers of metalliferous sediments. There is no correlation between the contents of these minerals and the contents of basalt fragments including the altered ones. The volcanic material in the TAG hydrothermal field has ages as dated of ~27 ka, ~18 ka, and 8–10 ka (Bogdanov et al. 1992, 1994). These data provide evidence of alternative stages of hydrothermal and volcanic activity and exhibit a cyclicity of these processes in periods of about 10 ka.

Following these studies materials were obtained on metalliferous sediments accumulated near the Mir Zone and Alvin Zone. These data are summarized in Fig. 5.2. The results of dating of the massive sulfide samples from the hydrothermal accumulations in the TAG hydrothermal field are shown as well. Synchronism in the stages of intensive accumulation of the metal-bearing matter in the sediments, regardless of the place of their

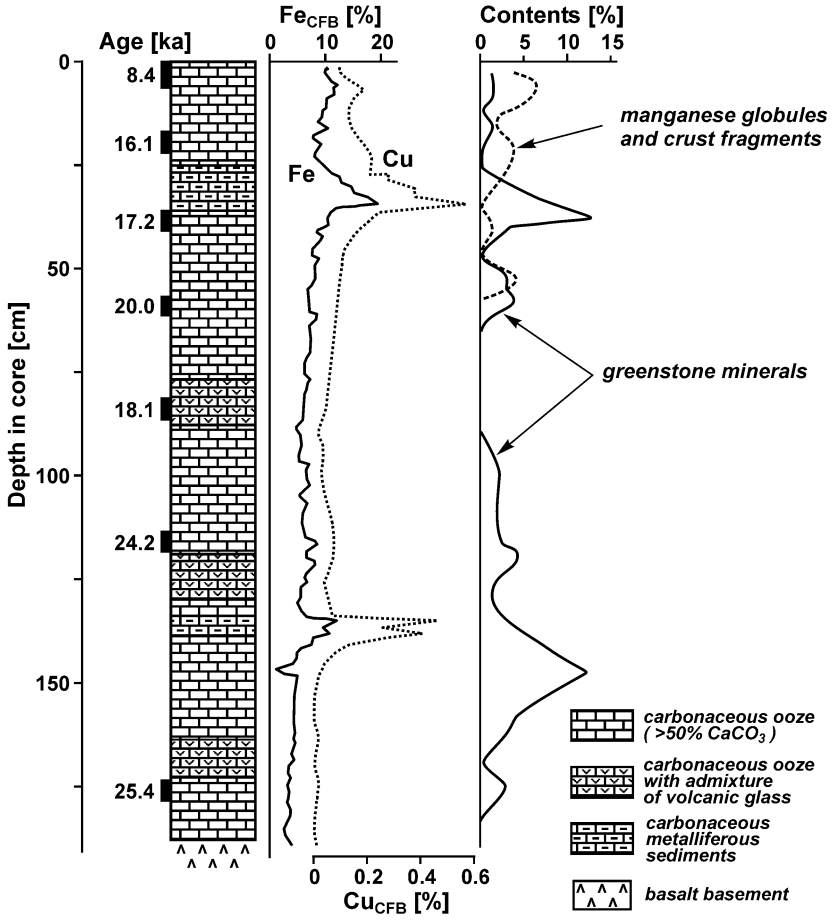

Fig. 5.1. Composition of bottom sediments in Core AMK-1785. Contents of greenstone minerals, manganese globules and crust fragments are shown in the sandy-silt grain size fraction of sediments. After Lisitzin et al. (1990).

deposition in relation to the massive hydrothermal accumulations, is evident at least in the last 25 ka. During this time there are three stages, ≥25–23 ka BP, 17–12 ka BP, and 7–3 ka BP, that demonstrate cyclicity within periods of ~10 ka. A reflection of the present phase of hydrothermal activity, which began ~100 years ago at the Active mound (Lalou et al. 1993), has not been found in the sediments collected nearby[39]. With an average sedimentation rate in the TAG hydrothermal field of ~2 cm ka^{-1}, a layer

[39] Presumably, it exists in sediments sampled in the cores collected directly on the Active mound (German et al. 1993). Unfortunately these sediments have not been dated.

about 2 mm thick would accumulate during this period of time, but with the common sampling methods in use, layers such as this are not detected or lost. On the other hand, within the TAG hydrothermal field the thickness of the layer in which mixing takes place due to bioturbation is about 6 cm (Kuptsov 1993). With the sedimentation rate of 2 cm ka^{-1} this thickness of sediments corresponds to a period of time of ~3 ka. For this reason, together with the less than ideal sampling methods, it has not been possible to identify the sediments accumulated during the final stage of high-temperature hydrothermal activity at the Mir mound. This stage ended about 700 years ago (Lalou et al. 1995; Fig. 5.2).

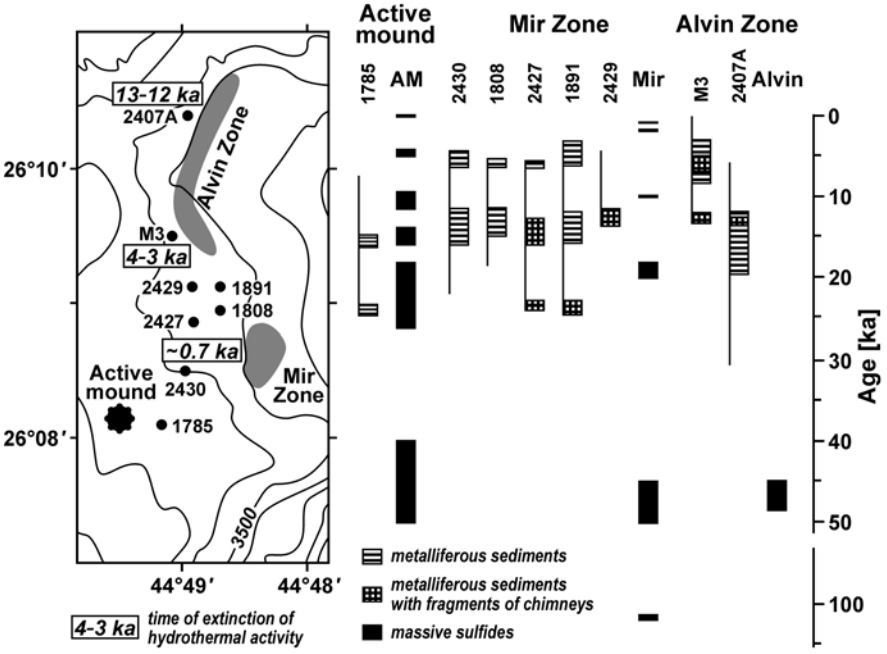

Fig. 5.2. Stages of intensive accumulation of the metal-bearing matter in sediments from cores collected at the TAG hydrothermal field and isotopic ages of samples of massive sulfides collected from hydrothermal accumulations. Cores AMK-1785, 1808, and 1891 were collected on Cruise 15 and Cores AMK-2407A, 2427, 2429, and 2430 on Cruise 23 of R/V *Akademik Mstislav Keldysh*. Data on these cores – materials of P.P. Shirshov Institute of Oceanology, data on Core M3 from Metz et al. (1988), data for the ages of the massive sulfides from Lalou et al. (1993, 1995).

There is another point to be considered. If at the Active mound the cyclicity of hydrothermal activity with a period of about 10 ka really exists, the next stage of activity should be in 3–7 ka. At present hydrothermal ac-

tivity and formation of mineral matter at the Active mound probably are depressed. The existence of mineral formation during the depressed stages of hydrothermal activity, that is not reflected or poorly reflected in sediments, can explain the existence of hydrothermal sulfide minerals that have ages that do not correspond to the ages of the mentioned stages of increased hydrothermal activity and the accumulation of the metal-bearing matter in the sediments (Fig. 5.2).

Gradual narrowing of the area of hydrothermal activity in the TAG hydrothermal field apparently has been taking place at least during the last 25 ka. The approximate time of extinction of hydrothermal activity in the Alvin Zone can be established from the data shown in Fig. 5.2. The synchronism in the stages of intensive accumulation of the metal-bearing matter in sediments, regardless of the place of their deposition relative to that of the massive hydrothermal deposits, is evidence of synchronism in the stages of hydrothermal activity. In the northern part of the Alvin Zone, based on the data from Core AMK-2407A, hydrothermal activity ceased 13–12 ka BP, and in the southern part, based on the data from Core M3, about 4–3 ka BP. The last stage of hydrothermal activity in the northern part is synchronous to the penultimate stage in the southern part of the zone. At the Mir mound hydrothermal activity became extinct about 700 years ago (Lalou et al. 1995). The gradual narrowing of the area of hydrothermal activity apparently results from the gradual reduction in the size of the magma chamber (Bogdanov 1997).

The history of hydrothermal activity and volcanism in the **Axial Seamount, Juan de Fuca Ridge**, during the last 35 ka has been reconstructed on the basis of data that show temporal variations in the occurrences of the indicators of volcanism and hydrothermal activity in the sediments that accumulated in the area of this seamount (Fig. 5.3) and on temporal variations in the accumulation rate of hydrothermal Fe (Fig. 1.43). This is summarized in Fig. 5.4 and described on the results of the investigations of Bogdanov et al. (1990) and Lisitzin et al. (1990).

The Axial Seamount is located immediately above the Cobb hot spot (Desonie and Duncan 1990). A volcanic body of the Axial Seamount formed when this hot spot was close to or near the spreading axis of the Juan de Fuca Ridge. However, the first complex group of effusive rocks dated >30 ka BP (Lisitzin et al. 1990) presumably formed on the flank of the rift zone; at that time the axis of the Juan de Fuca Ridge was not located above the Cobb hot spot.

In the period *from 30 to 20 ka BP*, following the termination of the first stage of volcanism, the mount located adjacent to the tectonic zone of the spreading ridge was dissected by a system of fissures. Channel ways were formed for the metal-bearing hydrothermal fluids and steady hydrothermal

circulation developed. Massive hydrothermal deposits were formed on the surface of the mount at the orifices of hydrothermal discharge and metalliferous sediments accumulated around the hydrothermal field.

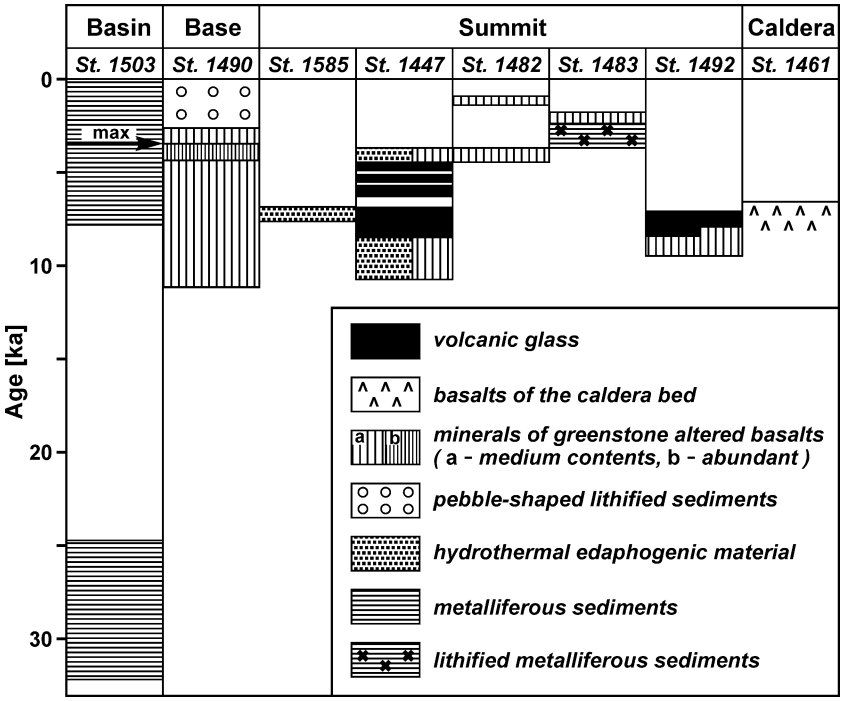

Fig. 5.3. Temporal variations in the occurrence of the indicators of volcanism and hydrothermal activity in sediment from the area of the Axial Seamount. After Bogdanov (1990a).

From 12 to 7 ka BP, hydrothermal activity was terminated almost completely. Basalt rocks blanketed and overlapped the volcanic complex of the mount and the hydrothermal bodies that had formed earlier. After the voiding of a magmatic chamber a collapse caldera formed. This stage of volcanism, presumably, was associated with a new geologic setting when the spreading center of the Juan de Fuca Ridge intersected the Axial Seamount.

From 6 to 3 ka BP the next active stage of hydrothermal activity occurred; but it was less intensive than the previous one.

In the period *from 2 to 0 ka BP*, there was a stage of caldera volcanism that was associated with the spreading of the plates; the spreading axis intersected the central part of the caldera. Hydrothermal activity of low intensity developed at the periphery of the caldera along the fault zones that formed the caldera. There is a decline at the present time in hydrothermal

discharge following the eruptions and volcanic activity on the seafloor at the Axial Seamount as observed by Baker et al. (2004).

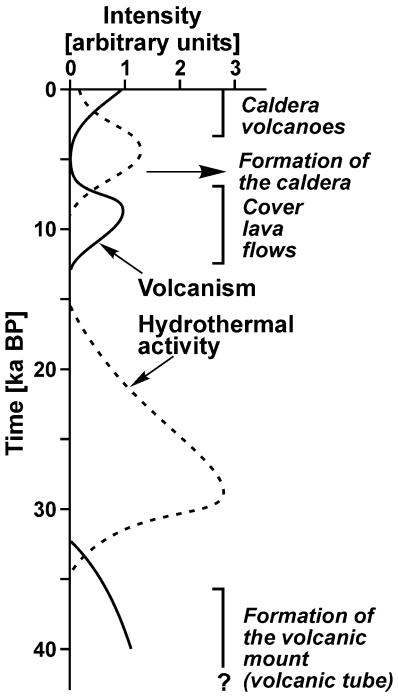

Fig. 5.4. Temporal variations of volcanism and hydrothermal activity at the Axial Seamount. After Lisitzin et al. (1990) with some changes.

The history of hydrothermal activity in the **southern part of the Juan de Fuca Ridge** can be reconstructed on the results of studies of the metalliferous sediments in Core KC-1 (44°44.21'N, 30°33.38'W, depth 2635 m) that accumulated during the last 130 ka (Olivarez and Owen 1989).

The core was collected 15.6 km west of the Juan de Fuca Ridge axis. With a half-rate of spreading of 3 cm a^{-1} during the past 130 ka the distance from the place of accumulation of the oldest sediments in the core to the ridge axis increased by 3.9 km; i.e. the oldest sediments accumulated 11.7 km from the axis. Factor analysis has been carried out for ascertaining the different sources of chemical elements in the sediments (Olivarez and Owen 1989). The relative contents of proximal and distal[40] hydrothermal

[40] These terms used by Olivarez and Owen (1989) have another meaning than the meaning used in this book, because sediments in the core have accumulated far from and outside of hydrothermal fields (or a field).

components in the detrital-free material have been calculated. The proximal component is enriched in Fe, distal component in Ba, Co, Mn, Ni, and REE. The relative contents of the components have varied with time. In general, in the more ancient sediments accumulated closer to the ridge axis the amount of the proximal component is higher (Fig. 5.5).

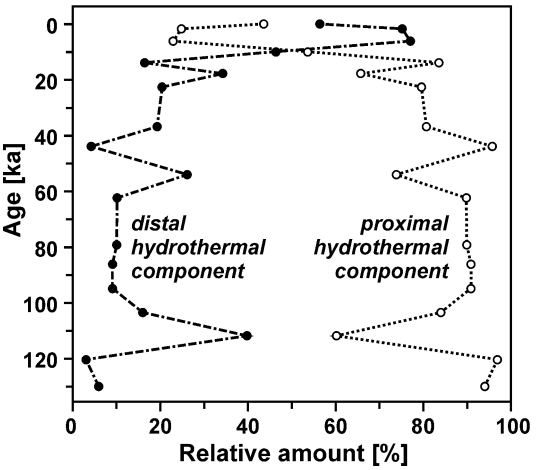

Fig. 5.5. Temporal variations in the relative amounts of proximal and distal hydrothermal components in detrital-free matter of sediments from Core KC-1. Based on data from Olivarez and Owen (1989).

Temporal variations in the accumulation rate of hydrothermal Fe (Fe_h*) in the sediments from Core KC-1 estimated on the data from Olivarez and Owen (1989) are shown in Fig. 5.6. These values are considerably lower than those observed at similar distances from the EPR axis (Boström 1973; Shimmield and Price 1988; Lisitzin et al 1990; Dekov 1994, et al.). In the 130 ka that transpired during the accumulation of the sediments collected in the core the distance of the place of their deposition from the Juan de Fuca Ridge axis increased from 11.7 km to 15.6 km (Fig. 5.6).

A general trend in the temporal variations of Fe_h* exhibits a decrease with decreasing sediment age and an increase in the distance of their deposition place from the ridge axis (Fig. 5.6). If the intensity of hydrothermal activity during the time of sediment deposition and other factors influencing the accumulation of hydrothermal matter, except for the distance of the deposition place from the ridge axis, remained constant and invariable, the value of the Fe_h* would gradually decrease with decreasing age of the sediments because of the increasing distance of the sediment deposition from hydrothermal vents.

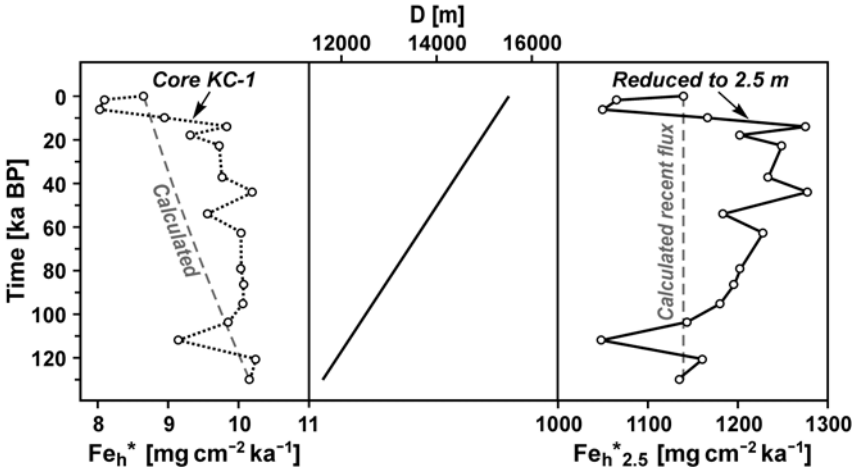

Fig. 5.6. Temporal variations in the distance from the deposition (D) place to the axis of the Juan de Fuca Ridge for sediments collected in Core KC-1, and for Fe_h* estimated from the data of Olivarez and Owen (1989) in comparison with Fe_h* variation calculated from the equation (4.1), $lg(Fe_h*/Fe_h*_{2.5}) = 0.23 – 0.56lgD$, for the value of Fe_h* at the top of the core, as well as calculated values of Fe_h* reduced to the distance of 2.5 m from hydrothermal vents.

Comparison of the data from Core KC-1 is shown in Fig. 5.6 with variation in the settling flux of the hydrothermal Fe that is related to the increasing distance from the axis, as calculated from the empirical equation (4.1) $lg(Fe_h*/Fe_h*_{2.5}) = 0.23 – 0.56lgD$ (see Sect. 4.4), with the value of Fe_h* observed in the upper part of the core or at a distance of 15600 m from the ridge axis. There is good agreement of the general trend of the values for Fe_h* in the core with those in the curve calculated from the equation (4.1). This agreement enables the estimation of the values of Fe_h* near hydrothermal vents during the last 130 ka by using the equation (4.1) and values for Fe_h* that have been calculated for the distance 2.5 m from hydrothermal vents. They are plotted in Fig. 5.6 and show that during this time the settling flux of the hydrothermal Fe near the vents varied little and was from ~1000 to ~1300 mg cm^{-2} ka^{-1}. These values are higher than those calculated for the North Cleft segment of the Juan de Fuca Ridge but lower than those for hydrothermal fields in the Endeavor Ridge and 13°N EPR areas, as well as for the Rainbow and Broken Spur hydrothermal fields (Fig. 4.26). Temporal variations of the $Fe_h*_{2.5}$ values show that ~130, 120, 105, and 10 ka BP the hydrothermal activity at the ridge axis was similar to that in recent times. From 120 to 105 ka BP and from 10 to 1 ka BP it was lower than the recent activity, and in an interval from 105 to 10 ka BP it was higher than the recent activity. During the intervals of time when

there was an increase in the intensity of hydrothermal activity there was a relative increase in the amount of the proximal hydrothermal component (Fig. 5.5).

The history of volcanic and hydrothermal activity in **the vicinity of the Rodriguez Triple Junction** in the Indian Ocean has been studied by Kuhn et al. (2000), using data for samples analyzed from the sediment cores collected in the central valley and in the vicinity of the Central Indian Ridge axis and in the vicinity of the Southeast Indian Ridge axis (Fig. 5.7).

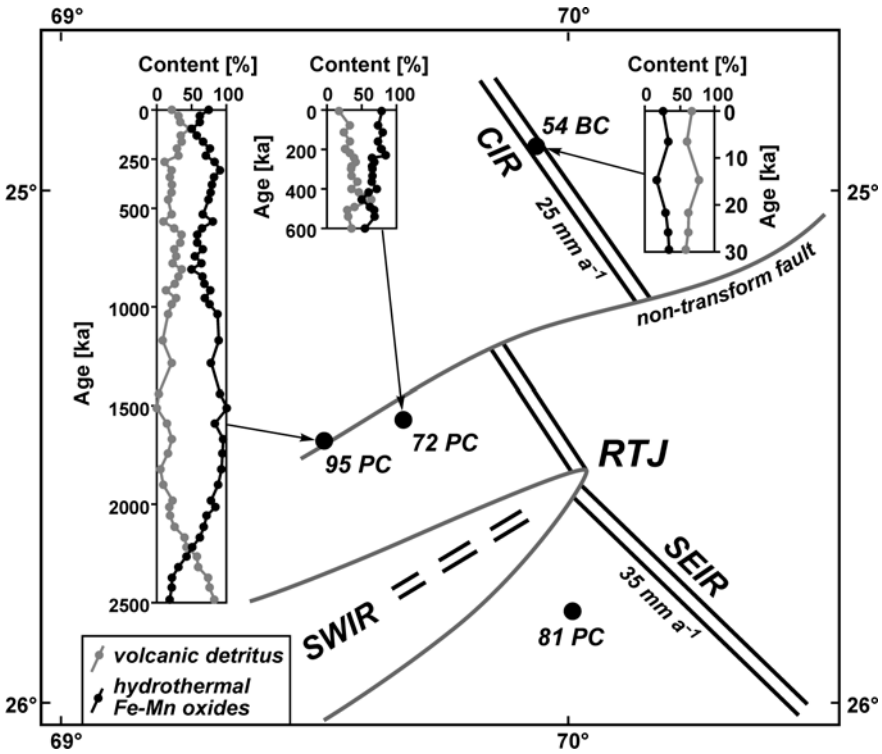

Fig. 5.7. Locations of the cores in the area of the Rodriguez Triple Junction (RTJ) and temporal variations in the relative contents of the volcanic detritus and hydrothermal Fe-Mn oxide end-members. CIR – Central Indian Ridge, SEIR – Southeast Indian Ridge, SWIR – Southwest Indian Ridge. 25 mm a^{-1} and 35 mm a^{-1} – half-rates of spreading for CIR and SEIR respectively. Compiled from Kuhn et al. (2000).

Multivariant analysis of the carbonate-free contents of Si, Al, Ti, Mg, K, Fe, Mn, Cu, Zn, and Ni has shown that the sediments that have accumulated in the vicinity of the Rodriguez Triple Junction consist of two main end-members that are mixed in different proportions in the samples stu-

died. The first end-member consists of volcanic detrital components and the second of hydrothermal Fe-Mn oxides. Temporal variations in the relative contents of these end-members in the sediments that have been dated are shown in Fig. 5.7. In spite of the high relative contents of the hydrothermal Fe-Mn oxide end-member, the accumulation of both end-members in the cores from the axial zone of the Central Indian Ridge (Cores 95 PC and 72 PC) reflect the evolution of a non-transform fault that separates the first and second Central Indian Ridge segments rather than the history of the spreading axis. Data from Core 81 PC reflect magmatic-volcanic activity of the rift axis (Kuhn et al. 2000).

Temporal variations in the Fe_h* in the sediment that has been dated from Core 81 PC estimated on the data from Kuhn et al. (2000) are shown in Fig. 5.8, and data for the background sediments have been taken from Table 1.5. During the last 520–530 ka while these sediments accumulated the distance from the place of their deposition to the Southeast Indian Ridge axis increased from 1.0 km to 19.5 km (Fig. 5.8).

A general trend in the temporal variations of Fe_h* in sediments from Core 81 PC exhibits a decrease with decreasing sediment age and increasing distance of their deposition from the ridge axis. A best fit equation for the relationship of the Fe_h* and the distance data is:

$$\lg Fe_h^* = 2.96 - 0.57 \lg D.$$

The correlation coefficient is high (R=0.88) in spite of the temporal fluctuations in the Fe_h* values relative to the general trend (Fig. 5.8).

It follows from this equation that the value of $Fe_h^*_{2.5}$ for the best-fit relationship is 541 mg cm^{-2} ka^{-1}. Using this value the equation can be got:

$$\lg(Fe_h^*/Fe_h^*_{2.5}) = \lg Fe_h^* - Fe_h^*_{2.5} = 2.96 - 0.57\lg D - \lg 541 =$$

$$= 0.23 - 0.57\lg D.$$

This equation is practically the same as the empirical equation (4.1),

$$\lg(Fe_h^*/Fe_h^*_{2.5}) = 0.23 - 0.56\lg D,$$

that shows the relative decrease of Fe_h* with increasing distance from hydrothermal vents in the Pacific Ocean (Sect. 4.4). The equation can be used for estimating Fe_h* values near hydrothermal vents in the past 520–530 ka. The values of Fe_h* reduced to the distance of 2.5 m from the vents have been calculated. They are plotted in Fig. 5.8 and show that during this time the settling flux of the hydrothermal Fe near the vents varied from ~300 to ~900 mg cm^{-2} ka^{-1}. These values are higher than those for the North Cleft segment of the Juan de Fuca Ridge but lower than those for the southern part of the Juan de Fuca Ridge (Fig. 5.6) and for hydrothermal fields of the

Endeavor Ridge and 13°N EPR, as well as for the Rainbow and Broken Spur hydrothermal fields (Fig. 4.26).

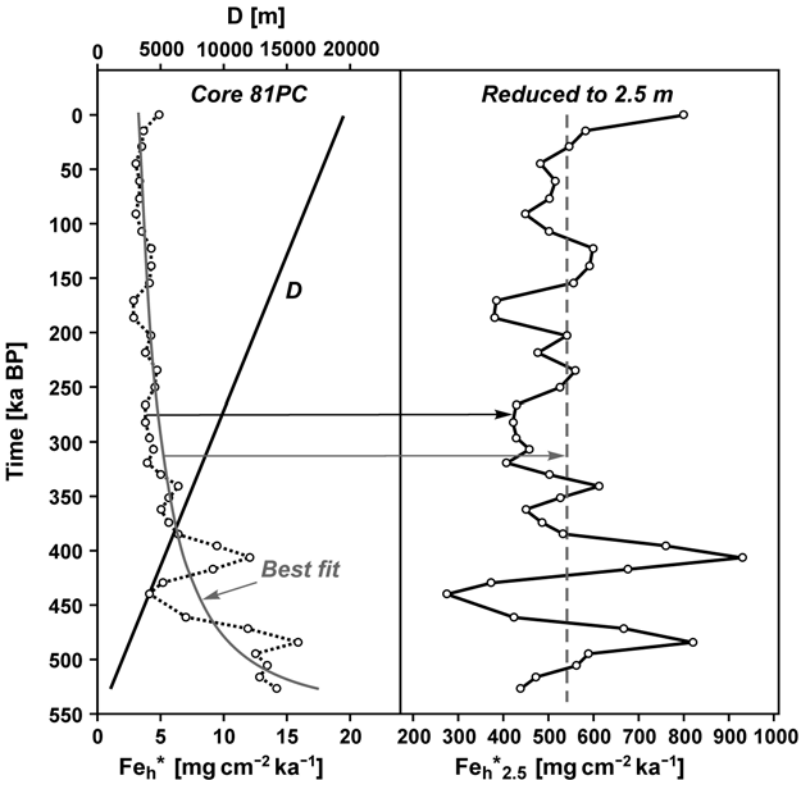

Fig. 5.8. Temporal variations in the distance of the deposition (D) from the axis of the Southeast Indian Ridge for sediments in Core 81 PC, and of Fe_h* estimated from the data of Kuhn et al. (2000) in comparison with variation in Fe_h* calculated from the best fit equation $lgFe_h^* = 2.96 – 0.57lgD$, as well as calculated values of Fe_h* reduced to the distance of 2.5 m from hydrothermal vents.

Temporal variations in the $Fe_h^*{}_{2.5}$ values show that in the periods of time 480 to 490 and 400 to 410 ka BP and in recent time there were stages of increased hydrothermal activity when the values of the $Fe_h^*{}_{2.5}$ exceeded 800 mg cm^{-2} ka^{-1} and the lowest value, <300 mg cm^{-2} ka^{-1}, was ~440 ka BP. During most of the time recorded in Core 81 PC the $Fe_h^*{}_{2.5}$ value varied from ~400 to ~600 mg cm^{-2} ka^{-1}. The variations in the $Fe_h^*{}_{2.5}$ value are quasicyclic with the duration of most of the cycles from 60 to 80 ka. Presumably, cycles with shorter periods also exist, like those on the EPR (Fig. 1.16), at Axial Seamount (Fig. 5.4) or in the TAG hydrothermal field (Fig. 5.2), but shorter intervals between samples are needed for their detection.

The estimations of the $Fe_h*_{2.5}$ values have been based on the assumption that the distances from the points of sediment deposition to the ridge axes are equal to the distances from the hydrothermal vents. More often the distances of the deposition points of the sediments in the cores to the axes are shorter than the distances to the vents, especially where the distances are not known for the ancient or proposed hydrothermal vents or fields that we are dealing with. In this case apparently some of the results obtained are underestimated somewhat including those based on data from Cores KC-1 and 81 PC. The use of two or more cores of sediments containing hydrothermal matter derived from one source should increase the accuracy of the estimated values.

The history of hydrothermal activity and mineral formation along **the East Pacific Rise axis between 20°30'S and 22°00'S** in the last 50 ka has been reconstructed using data of the study of 10 sediment cores that were collected 20 km to the west of the EPR axis.

This part of the EPR axis is one of the most hydrothermally active areas in the World Ocean. The temporal cyclicity of hydrothermal activity in this area was mentioned in Sect. 1.1.4. and was recognized by Dekov (1994) in the composition of the metalliferous sediments in three sections 10, 20, and 40 km west of the EPR axis. The amplitude of the variation in the contents of Fe_{CFB} is somewhat low, on the average about 10 percent relative to the contents. Obviously the low amplitude is caused by the high hydrothermal background related to the permanent existence of hydrothermal activity at some place or other, or simultaneously at places in the part of the EPR axis being considered or in adjacent parts. The contribution of hydrothermal matter from the adjacent neighboring sites that are in different stages of hydrothermal activity may result in the interference of their hydrothermal signals. Nevertheless, Fourier analysis carried out on materials in the study of 1524 samples have made it possible to demonstrate that more than half of the cycles detected had periods of 10±5 ka (Dekov 1994). This has not only provided evidence of the existence of cyclicity in the hydrothermal activity in individual hydrothermal fields but also has shown that information for individual hydrothermal fields can be extracted from integral indicators of the hydrothermal activity in the metalliferous sediments that accumulated at least as far as 40 km from the EPR axis.

Studies of metalliferous and transitional sediments collected along sections parallel or subparallel to a spreading axis enable the reconstruction of the history of hydrothermal activity within separate segments of a spreading ridge. The analysis of isopleths of the accumulation rate of hydrothermal Fe in spatiotemporal dissection is a very productive approach to these reconstructions.

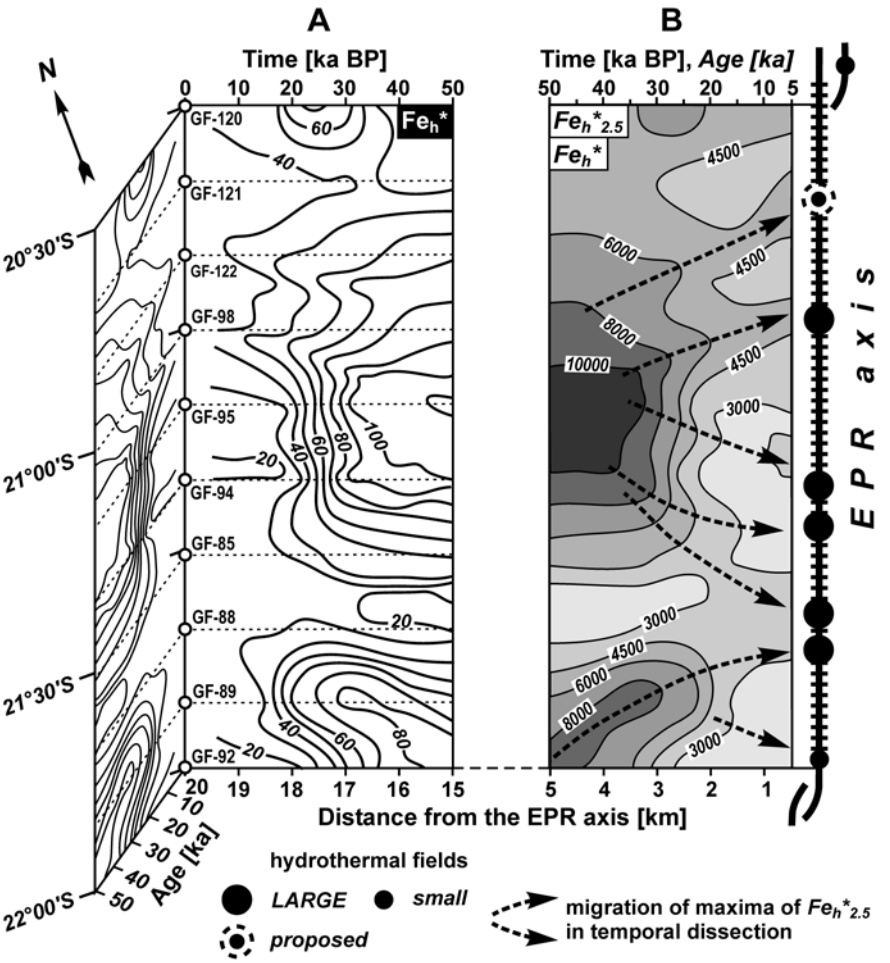

Fig. 5.9. A – Temporal evolution of Fe_h* [mg cm^{-2} ka^{-1}] in surface metalliferous sediments in the last 50 ka along a section parallel to the EPR axis and gradually moving to the west from the axis with the half-rate of spreading of 10 cm a^{-1}. After Dekov (1994) with changes and additions. B – Reconstruction of Fe_h*$_{2.5}$ [mg cm^{-2} ka^{-1}] for the last 50 ka and the distribution of Fe_h* [mg cm^{-2} ka^{-1}] in the lowermost sediments of the metalliferous stratum within 5 km to the west of the EPR axis.

Following my advice and recommendations, Dekov (1994) plotted his data for the accumulation rates of hydrothermal Fe in sediments of the section mentioned that is 20 km west of the EPR axis in spatiotemporal dissection and obtained a scheme of the evolution of Fe_h* in the surface metalliferous sediments in the section during the last 50 ka (Fig. 5.9A). It was based on the assumption that the half-rate of spreading of the EPR in this

area was equal to that at 20°S, which is about 10 cm a^{-1} (Rea 1978), and 5 km of the Pacific plate motion corresponds to a time interval of 50 ka at this half-rate of spreading.

Based on these data for the distribution of Fe_h* in the surface metalliferous sediments of this moving section, the values of $Fe_h*_{2.5}$ have been reconstructed (Fig. 5.9B) by using the equation (4.1), $lg(Fe_h*/Fe_h*_{2.5}) = 0.23 - 0.56lgD$, that shows the relative decrease of Fe_h* with increasing distance from hydrothermal vents in the Pacific Ocean (Sect. 4.4). Corrections for the westerly direction of bottom currents in this area were calculated and applied from the data of Walter and Stoffers (1985) and Gurvich (1998). In this reconstruction as well as in previous ones (Fig. 5.6, 5.8) it was assumed that: a) the hydrothermal Fe has been contributed to the sediments only from hydrothermal plumes or their fragments; and b) the accumulation rate of the hydrothermal Fe at the time of deposition of the sediments was equal to its settling flux.

At present the sediments that accumulated at the EPR axis 50 ka BP are located 5 km to the west and east of the axis because of the spreading; the half-rate of spreading is 10 cm a^{-1} (or 0.1 km ka^{-1}). Therefore the plot in Fig. 5.9B shows not only the evolution of the settling flux of the hydrothermal Fe at distance of 2.5 m from the hydrothermal vents during the last 50 ka, but it is also a reconstruction of the distribution of Fe_h* in the lowermost part of the metalliferous stratum within 5 km to the west of the EPR axis.

During the last 50 ka the reconstructed settling flux of the hydrothermal Fe along the EPR axis between 20°30'S and 22°00'S decreased to approximately half of the initial value (Fig. 5.9B). From 50 to 40 ka BP the average value of $Fe_h*_{2.5}$ was ~7000 mg cm^{-2} ka^{-1}, from 40 to 30 ka BP it was ~6900 mg cm^{-2} ka^{-1}, from 30 to 20 ka BP it was 5200 mg cm^{-2} ka^{-1}, from 20 to 10 ka BP it was ~3700 mg cm^{-2} ka^{-1}, and from 10 to 5 ka BP it was ~3600 mg cm^{-2} ka^{-1}. Apparently the general intensities of hydrothermal activity and mineral formation along the EPR axis between 20°30'S and 22°00'S followed a similar trend.

The reconstructed values of $Fe_h*_{2.5}$ are similar or higher than settling fluxes of the hydrothermal Fe reduced to 2.5 m from hydrothermal vents for the hydrothermal fields of the Endeavor Ridge and 13°N EPR, and lower than those for the Rainbow and Broken Spur hydrothermal fields (Fig. 4.26). The maximal reconstructed values of $Fe_h*_{2.5}$, ~15000 mg cm^{-2} ka^{-1}, are similar to the settling fluxes of the hydrothermal Fe reduced to 2.5 m from the vents of the Rainbow and Broken Spur hydrothermal fields.

High values of the settling fluxes of the hydrothermal Fe in the mentioned hydrothermal fields are of very local distribution. And the reconstructed average values of $Fe_h*_{2.5}$ characterize the segment ~160 km long. The set-

tling flux of the hydrothermal Fe near individual vents can be lower, similar or higher than near the vents in the Rainbow and Broken Spur fields. But the reconstructed values of $Fe_h*_{2.5}$ for the segment ~160 km long can be explained only by a great number of hydrothermal vents. This agrees well with the conclusions from studies of the non-buoyant hydrothermal plumes (Sect. 4.3.2).

Fig. 5.9B enables the reconstruction of the position and migration of the sites of hydrothermal activity on the EPR axis between 20°30'S and 22°S for the last 50 ka. Temporal migration of the sites is reflected by the temporal migration of the maxima of the $Fe_h*_{2.5}$ values.

By using the temporal dissection method these can be shown as trajectories. Reconstruction of the recent sites of hydrothermal activity is the least accurate because of the accumulation of the youngest sediments in the cores at a maximum distance from the EPR axis (Fig. 5.9A). Nevertheless this reconstruction shows that the reconstructed positions of the recent sites agree well with the locations of the existing hydrothermal fields (Fig. 5.9B). This evidence shows that the reconstructions of the earlier positions are reasonably accurate.

According to the reconstruction of the history for the period from 50 to 30 ka BP, when hydrothermal activity had more than twice the intensity than in recent time, two main hydrothermal centers existed in the central and southern parts of the segment of the EPR axis that was studied. During this time the southern center was migrating to the north at the rate of ~1 m a^{-1} and in the period from 35 to 30 ka BP a gradual decrease in the hydrothermal activity in the central part of the segment and the splitting of this hydrothermal center began to take place. In the period from 30 to 20 ka BP the decrease in hydrothermal activity continued in the central and southern parts of the segment. The splitting of the hydrothermal center in the central part of the segment may have resulted in the existence of separate large hydrothermal fields; two fields of this group were migrating to the north at the rate of ~0.5 m a^{-1}, and three other fields were migrating to the south at the rates of 0.6–0.9 m a^{-1}. The migration of the southern center to the north continued at the rate of ~0.6 cm a^{-1}. From 20 ka BP until recent time the intensity of the hydrothermal activity was much lower than earlier and did not vary significantly. During this time the migration of the fields in the central group to the north continued at the same rate, and the rate of migration of the southern fields in the group decreased. The migration of the southern center to the north continued at a lower rate of ~0.3 m a^{-1}. Presumably, a new hydrothermal field that resulted from the splitting of the southern center appeared in the southern part of the segment. This field migrated to the south.

The pattern of migration of the maximum values for $Fe_h*_{2.5}$ that were used for the reconstruction of hydrothermal activity cannot be explained by the movement of the ocean crust or by bottom currents. It is next to impossible for: a) close parts of a lithosphere plate to move at the rate of n·10 cm a^{-1} in the opposite directions; and b) during many thousands of years the directions of the bottom currents in adjacent areas of a deep ocean would differ as much as the directions of the migration of the maximum values for $Fe_h*_{2.5}$, or even cross each other.

High values of the settling flux and the accumulation rate of the hydrothermal Fe in sediments usually accompany the formation of large or numerous small massive sulfide bodies at the hydrothermal orifices (Lisitzin et al. 1990). It is certainly within reason to suggest that, at the active stage in the life of high-temperature hydrothermal vents that are accompanied by the formation of metalliferous sediments, the settling flux and the accumulation rate of the hydrothermal Fe in the vicinity of the hydrothermal vents on an axis of a spreading ridge reflect the rate of formation of massive sulfides. If this is the case the diagram in Fig. 5.9B also reflects the present occurrence of hydrothermal sulfide mineral masses (if they are preserved) that formed on the EPR axis between 20°30'S and 22°00'S during the last 50 ka and located to the west of it at distances up to 5 km. The characteristics of the relationship of the settling flux or the accumulation rate of the hydrothermal Fe on an axis of a spreading ridge near hydrothermal vents and the occurrence of masses of hydrothermal sulfide minerals probably vary along the rift systems in the World Ocean. It is expected that this relationship will be better defined in the future.

5.2. Reconstruction of the history of hydrothermal activity and mineral formation based on the studies of deep-sea drilling cores

The accumulation rate of the hydrothermal metal-bearing matter in sediments is a very useful parameter for reconstructing the intensity of hydrothermal activity and mineral formation in the geological past. The values of this parameter in sediments collected during the deep-sea drilling program vary from place to place and along the cores. Usually the sediments in the lower parts of the cores accumulated earlier and closer to the spreading axes than the overlying sediments. Therefore on comparisons of the values measured even in one core and especially in many cores, techniques of systematizing and consideration of these data are of great importance. Certainly the best way to analyze and study the temporal variations in the ac-

cumulation rates of the hydrothermal metal-bearing matter in sediments is to do detailed palinspastic mapping for the chosen time intervals both in separate areas and in the whole ocean. However, such studies of the ocean floor require detailed information and data that are available only from the analyses of many samples from many drill cores. Obtaining this kind of data is laborious and expensive, and is not likely to be possible now or in the near future. Data and work of this kind has been made possible for the study of recent stages in geologic history in only one area of metalliferous sediments in the Southeast Pacific.

The following kinds of studies are possible at the present time: 1) studies of variations in the accumulation rates of the hydrothermal metal-bearing matter in sediments from sections or narrow strip-sections along spreading tracks or along perpendiculars to the axes of spreading ridges, and 2) studies of variations in the accumulation rates of the hydrothermal metal-bearing matter in sediments from sections parallel or subparallel to the axes of spreading ridges.

The first kind of studies was attempted earlier by Boström (1973), Gurvich et al. (1984), Lyle et al. (1986). However, the analysis of the evolution of the hydrothermal activity was complicated in these studies because temporal variations in the distances of the points of sediment deposition to the spreading axes were not taken into account, and these distances for the sediments could vary in each core from zero to many hundreds of kilometers. This omission can be avoided by systematizing the data in relation to temporal coordinates and by plotting the age of the samples on the ordinate axes and the time since the beginning of the formation of strata on the abscissa axes. In this case, if the scales of both axes are equal, the sequence of the data for each core falls on a straight line that is at an angle of 45° to the ordinate axis. The point where this line crosses the ordinate axis corresponds to the age of the sediments that lie directly on the basalt basement and the point where this line crosses the abscissa axis shows the duration of time for the accumulation of the whole sedimentary series in the place where the core was collected. The line is not continuous if there are hiatuses in the strata and the breaks correspond to the times and duration of the hiatuses. Use of the temporal coordinates is convenient for comparing data from different sediment cores as: a) for the ordinate axis there is no need to consider differences in sedimentation rates between coeval sediments from different cores and differences in sedimentation rates in sediments accumulated at different times, and b) for the abscissa axis there is no need to consider differences in spreading rates at different times, if it is assumed here that in each moment of geologic time the spreading rate within a part of a spreading ridge crossed by a strip-section was identical.

For demonstrating this method strip-sections (or sections), usually not more than 10° to 15° in width, have been chosen in the southern and northern parts of the Pacific and Atlantic Oceans and the locations of the drill holes from these sections are shown in Fig. 3.3. Data for the accumulation rate of the hydrothermal Fe in the metalliferous and non-metalliferous sediments that have an admixture of the hydrothermal metal-bearing matter have been used.

The southern section in the Pacific Ocean is located west of the EPR axis between 19°S and ~6°S (Fig. 3.3) and in general its direction corresponds to the direction of the Pacific plate motion. The distribution of the values of Fe_h* in the sediments of this section in the temporal coordinates is shown in Fig. 5.10A. It covers the time period from 40 Ma BP to 0 Ma BP. During this period the values of Fe_h* varied over a wide range and maximum values occurred about 38–36, 25–24, 18, 14, 9–8, and 5 Ma BP.

Variations in the accumulation rates of hydrothermal Fe and Mn do not correlate with the variations in the spreading rate (Fig. 5.10A, 5.11). Only the maximum values for Fe_h* indicated at ~5 Ma BP and 38–36 Ma BP may have resulted from increases in the spreading rate. The increase at ~5 Ma BP can be seen in Fig. 5.11. As for the increase at 38–36 Ma BP, according to Zonenshain and Khain (1989), the average rate of crust accretion in Eocene time for the Pacific Ocean was almost one and a half times higher than at present. The period of time from 33–32.5 Ma BP to 46–44.5 Ma BP is characterized by increased values of a relative momentary spreading rate[41] in the Pacific Ocean (Schreider 1982).

The maxima of values for Fe_h* in sediments accumulated ~27–25, 18, 14, and 9–8 Ma BP (Fig. 5.10A) are synchronous with the earlier measured maxima of values for the accumulation rate of Mn (Lyle et al. 1986, 1987). They correlate with events of tectonic reorganizations in the Southeast Pacific (Lyle et al. 1986, 1987; Rea and Leinen 1986). The maximum at ~25 Ma BP apparently is synchronous with the formation of the rift between the Cocos and Nazca plates, 25–23 Ma BP, as well as with the jump of the spreading center 175 km to the west, from the Selkirk Ridge segment of an ancient spreading ridge to the EPR in the period from 24 to 22 Ma BP (Mammerickx et al. 1980). The maximum at ~18 Ma BP apparently is synchronous with the spreading center jump 500 km to the west, from the Mendoza Rise segment of an ancient spreading ridge to the EPR, that took place 20–18.5 Ma BP. At approximately the same time the jumps

[41] Ratio of the linear spreading rate measured between two adjacent magnetic anomalies in a profile to the spreading rate measured between two foregoing magnetic anomalies at the same profile.

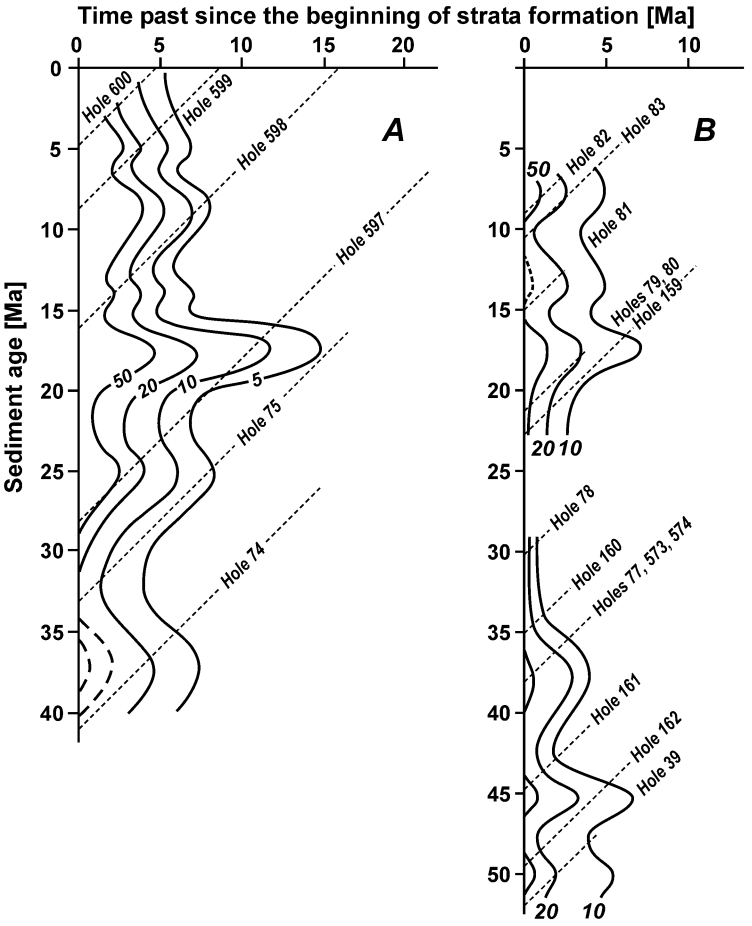

Fig. 5.10. Distribution of Fe_h* [mg cm^{-2} ka^{-1}] in bottom sediments of the southern (A) and northern (B) sections in the Pacific Ocean.

westward took place from the Gallego Rise and Roggeveen Rise, the segments of ancient spreading ridges, to the EPR (Mammerickx et al. 1980). The maximum at ~14 Ma BP apparently is synchronous with the major southward jump of the Cocos–Nazca spreading center, that took place ~14.5 Ma BP (Werner et al. 2003) and with the existence at this time of two spreading centers, between the Galapagos and unnamed faults; they were the EPR and the parallel ridge about ~400 km to the west of it. About 11 Ma BP the parallel center became extinct (Mammerickx and Klitgord 1982). Apparently the maximum at 9–8 Ma BP resulted from the jump of the spreading center from the ancient Galapagos Rise to the EPR. Both ridges were active in the time interval from 8.2 to 6.5 Ma BP (Mammerickx

et al. 1980), and this is reflected clearly in the increase of the accumulation rate of the hydrothermal metal-bearing matter in the metalliferous sediments of DSDP Site 319 in the Bauer Depression (Dymond et al. 1977). And furthermore, between 10.5 and 8 Ma BP the Pacific-Riviera Ridge changed in strike direction from north-northwest to northeast (Lyle et al. 1986; Rea and Leinen 1986).

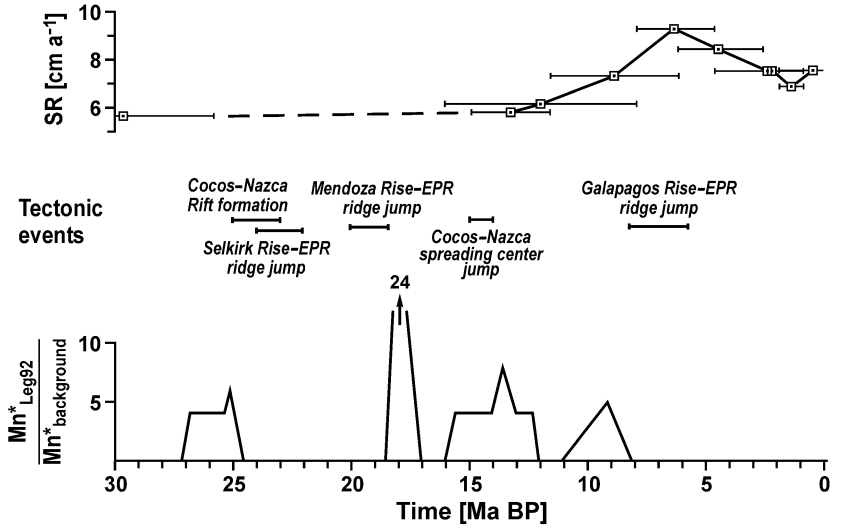

Fig. 5.11. Half-rate of spreading (SR) of the EPR at 19°S, periods of increased Mn accumulation rate (Mn*) in sediments collected in Leg 92 DSDP, and some tectonic events in the Southeast and Central East Pacific during the last 30 Ma. After Rea and Leinen (1986) with addition from Werner et al. (2003).

The maxima of values in the accumulation rates of the hydrothermal metal-bearing matter, mentioned earlier, that are synchronous with the events of tectonic reorganizations and especially the maximum ~18 Ma BP are significantly high (Fig. 5.10A). They cannot be explained by the decreasing distances from the sites of sediment deposition to spreading centers alone. Lyle et al. (1986, 1987) have assumed that breakings and changes in the strike of the ridges associated with the events of tectonic reorganizations could have increased the intensity of the hydrothermal activity substantially because of the fracturing of the ocean crust that enabled more active interaction of ocean water with hot rocks.

Based on the values of Fe_h* the temporal variations in the total accumulation of the hydrothermal Fe have been estimated in the sediments in the whole section within a band 1 km wide (Fe_{1km}). That is to say, estimates have been made of the temporal evolution in the contribution of hydrothermal Fe at ~19°S from 1 km of the rift length to the sediments located west

of the EPR axis. These estimated values reflect the evolution in the intensity of the hydrothermal activity and the mineral formation related to it. The resulting estimates are shown in Fig. 5.12A.

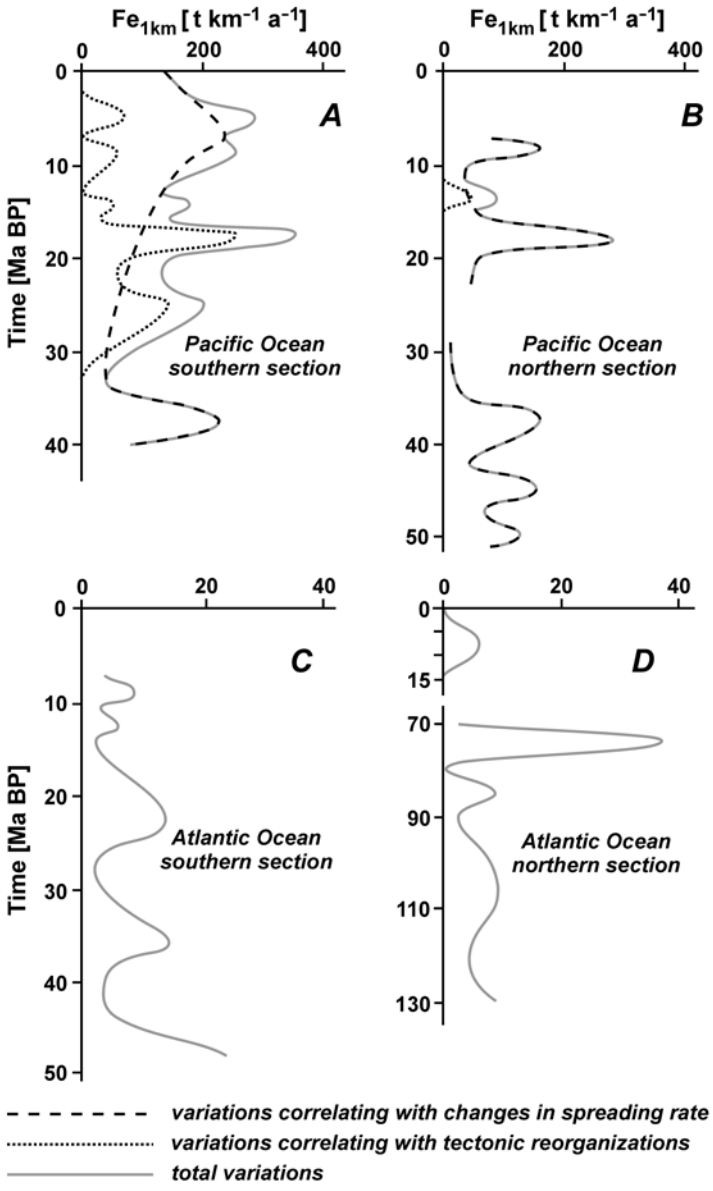

Fig. 5.12. Temporal variations of accumulation of hydrothermal Fe in sediments of the sections within bands 1 km wide along tracks of lithosphere plates.

The southern section is located to the west of the EPR axis within the field of recent metalliferous sediments in the Southeast Pacific. In the area around 19°S the value of Fe_{1km} for the recent metalliferous sediments is about 150 t km^{-1} a^{-1} (Fig. 5.12) which is comparable to the average value for the last 40 Ma. Within the field of the recent metalliferous sediments about 550000 tons of hydrothermal Fe accumulates annually (Table 1.2); and if the length of the rift within the field is ~4000 km the average value of Fe_{1km} for the two flanks of the EPR is about 140 t km^{-1} a^{-1}; for one flank it is about 70 t km^{-1} a^{-1}, which is less than twice that for the western flank of the ridge in the area around 19°S.

Most of the holes in **the northern section in the Pacific Ocean** have been located between 0° and 16°N (Fig. 3.3). Distribution of the values of Fe_h* in the basal sediments of this section in the temporal coordinates is shown in Fig. 5.10B. It covers the period of time from 52 to 6 Ma BP. Because of the lack of data there is a void from 29 to 23 Ma BP. In general the variations of Fe_h* are close to those for the section in the southern part of the Pacific Ocean. The maxima of values for Fe_h* occurred about ~50, 45, 39–37, 18–17, 14–13, and 8–7 Ma BP and all of the maxima or the grouping of them are synchronous with the periods of time and episodes when there was an increase in the average spreading rate of the North Pacific (Fig. 5.13). A long period in Eocene time, when there was an increase in the spreading rate, coincided with a period of time when there was an increase in the average spreading rate for the whole Pacific Ocean. In Eocene time the average rate of accretion of the Pacific crust was at a maximum for all of Cenozoic time (Zonenshain and Khain 1989). Presumably, the general increase in Fe_h* in the Eocene sediments of the section corresponds to this increase in the spreading rate, and there are maxima of Fe_h* at ~50, 45, and 39–37 Ma BP above the background of this increase. The maximum at ~45 Ma BP is synchronous with the increase in the spreading rate of 45–42 Ma BP (Schwan 1985). The maxima at 18–17 and 8–7 Ma BP are synchronous with episodes of sharp increases in the average spreading rate in the North Pacific dated about 18 and 8 Ma BP. Apparently the maximum at ~14–13 Ma BP is synchronous with the major southward jump of the Cocos–Nazca spreading center that occurred about 14.5 Ma BP (Werner et al. 2003). The synchronism of the maxima of Fe_h* at ~18–17 and 8–7 Ma BP in the sediments of the northern section with the maxima at ~18 and 9–8 Ma BP in the sediments of the southern section is worthy of notice (Fig. 5.10). Probably the tectonic reorganizations at or about this time that have been mentioned when considering the southern section could also have influenced the Fe_h* values in the sediments of the northern section.

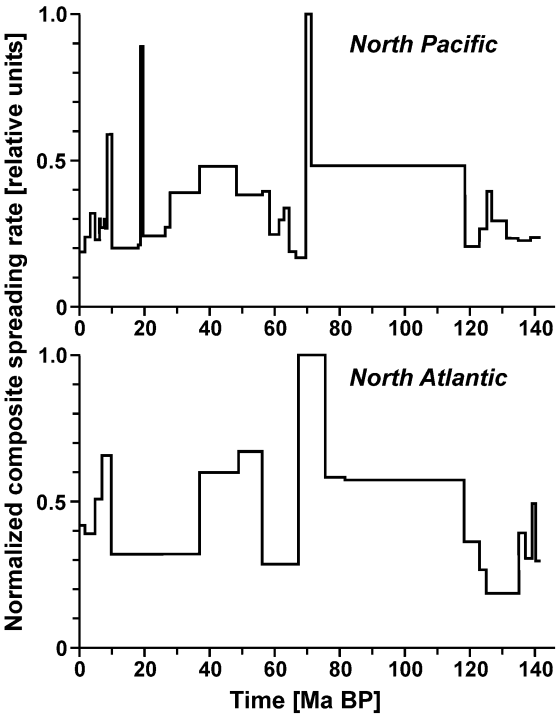

Fig. 5.13. Evolution of average normalized spreading rates for the North Pacific and the North Atlantic. Composed from Rich et al. (1986).

The values of Fe_{1km} in the sediments of the northern section to the west of the EPR axis have been estimated for the last 52 Ma (Fig. 5.12B). On the average these values are twice as low as those in the sediments of the southern section. Probably this is caused by a lower influence of tectonic reorganizations and slower spreading rates, at least in Neogene time. The general directions of the bottom currents may be another reason. At present, in the northern section area, an easterly direction of transport of the particulate hydrothermal matter is prevalent, and a westerly direction prevails in the southern section area (Lonsdale 1986; Lupton et al. 2004). Easterly and northeasterly directions of bottom currents have been prevalent in the northern section area at least since Eocene time (Lisitzin et al. 1980a).

An empirical relationship exists between the values of Fe_{1km} for the sections in the Pacific Ocean and the values of $Fe_h{}^*_{2.5}$ on the axis of the EPR:

$$Fe_h{}^*_{2.5} = 61Fe_{1km}, \qquad (5.1)$$

where $Fe_h{}^*_{2.5}$ is expressed as mg cm^{-2} ka^{-1}, and Fe_{1km} as t km^{-1} a^{-1}.

For the area crossed by the southern section near 19°S the value of Fe_{1km} for recent time is 140 t km^{-1} a^{-1} (Fig. 5.12). With this value of Fe_{1km} the value of $Fe_h*_{2.5}$ is ~8500 mg cm^{-2} ka^{-1}; with correction for the westerly bottom currents (Fig. 5.14) ~6000 mg cm^{-2} ka^{-1}. This value is close to the values of $Fe_h*_{2.5}$ as reconstructed between 20°30'S and 22°00'S in the last 50 ka (Fig. 5.9).

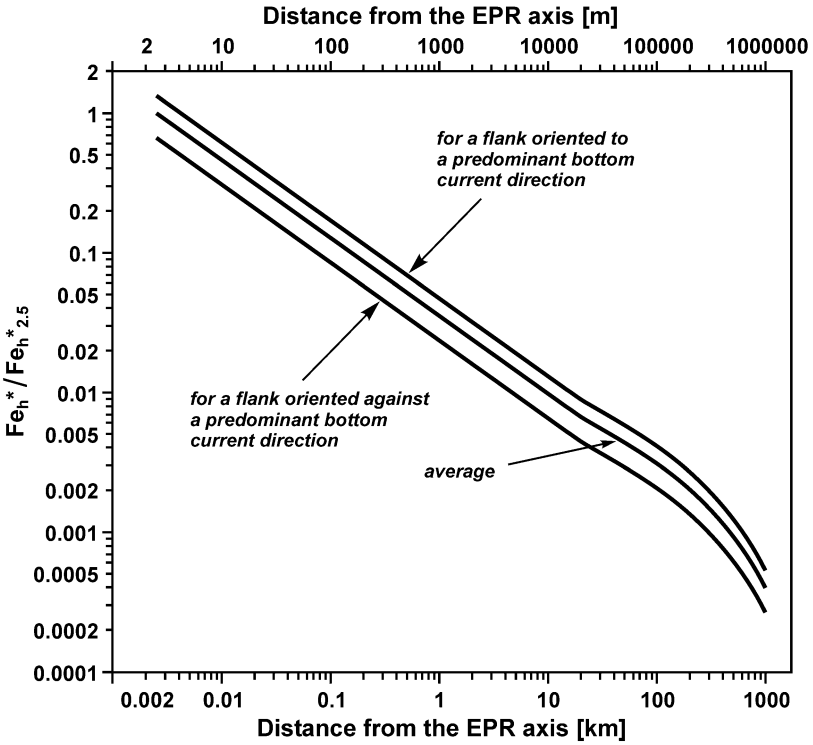

Fig. 5.14. Relative decrease in Fe_h* with distance in comparison with Fe_h* at 2.5 m from hydrothermal vents at different flank expositions and directions of bottom currents. Average for the field of recent metalliferous sediments in the Southeast Pacific and the East Pacific Rise between 5°S and 12°N.

The positions of holes of **the southern section in the Atlantic Ocean** are shown in Fig. 3.3. The section is located on the east and on the west sides of the Mid Atlantic Ridge axis between 30°S and 25°S. The distribution of the values of Fe_h* in the basal sediments of the section in the temporal coordinates is shown in Fig. 5.15A. It covers the time period from ~50 to ~6 Ma BP, and there are data that indicate that from ~66–65 Ma BP accumulation of the hydrothermal Fe in the basal sediments of the section was almost absent (Lisitzin et al. 1990). In general the values of Fe_h* in the

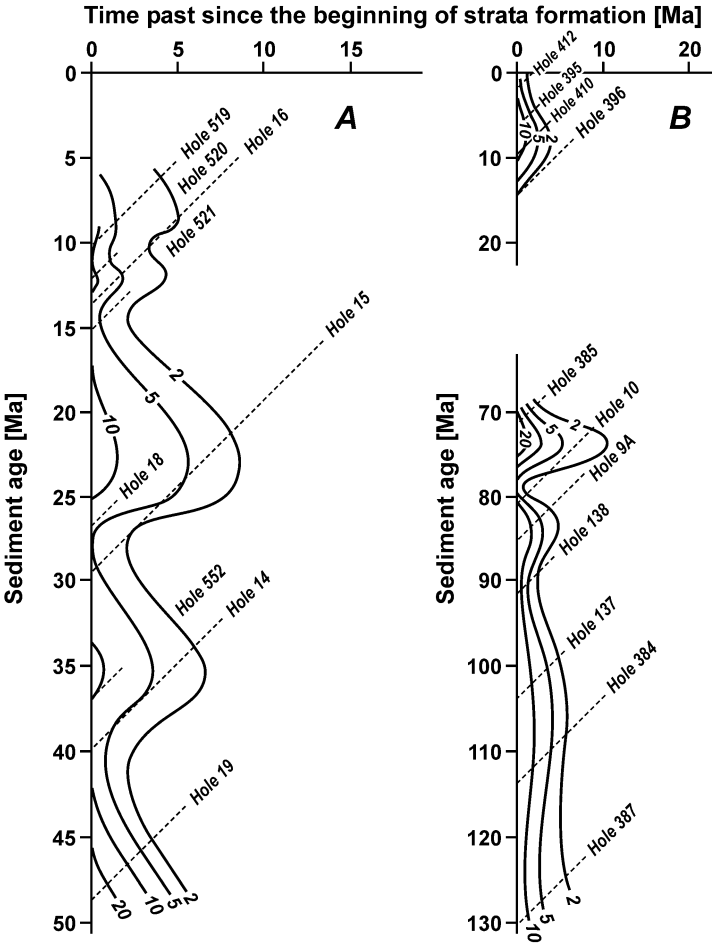

Fig. 5.15. Distribution of Fe_h* [mg cm^{-2} ka^{-1}] in bottom sediments of the southern (A) and northern (B) sections in the Atlantic Ocean.

sediments of the section are much lower than those in the sediments of the sections in the Pacific Ocean. During the time periods of ≥49, ~36–35, 24–20, ~12, and ~9–8 Ma BP there were maxima of the values of Fe_h*. The first and the third maxima are synchronous with the maxima of values of the accumulation rate of Mn in the basal sediments in the western part of the same section ~50–46 and 25–21 Ma BP (Boström 1973; Gurvich et al. 1984). Some of the maxima of the values of Fe_h* are synchronous with the maxima of the spreading rate. According to the data from Schreider (1985), the spreading rate was increasing during the time period from 59 to 52 Ma BP. Apparently the maximum for Fe_h* ≥49 Ma BP was synchrono-

us with the maximum in the spreading rate ~52 Ma BP. The spreading rate was also increasing during the time period from 42 to 38–37 Ma BP (Schreider 1985) and 38–35 Ma BP it began to decrease (Schwan 1985). The latter time interval was a period with a maximum spreading rate, and the maximum in the Fe_h* ~36–35 Ma BP apparently is synchronous with this maximum.

The positions of holes of **the northern section in the Atlantic Ocean,** located between 25°N and 45°N, are shown in Fig. 3.3. The distribution of the values of Fe_h* in the basal sediments of this section in the temporal coordinates is shown in Fig. 5.15B. It covers the periods of time from ~130 to ~70 Ma BP and from ~15 Ma BP to 0 Ma BP. In general the values of Fe_h* in the sediments of the section are close to the values in the southern section in the Atlantic Ocean. In the time period from 130 to ~70 Ma BP two maxima of the values of Fe_h* existed at ~85 Ma BP and 75–73 Ma BP. During the time interval from 130 to 100 Ma BP the values of Fe_h* did not vary significantly, but there are few data for this interval. Within the time period 15 to 0 Ma BP only one maximum occurs at ~8 Ma BP. Appreciable minima of the values of Fe_h* occurred at about 80–78, 70, and 15 Ma BP. These periods of time are in good agreement with those of decreasing spreading rates in the North Atlantic (Fig. 5.13). The highest values of Fe_h* were at ~75–73 Ma BP. This maximum was synchronous with the maximum in the spreading rate in the North Atlantic. The other maximum of Fe_h* at ~8 Ma BP was synchronous with another maximum in the spreading rate (Fig. 5.13). Only the average spreading rate is known for the whole period of time from 120 to 80 Ma BP and that is why comparisons for all parts of the period are not possible.

Variations in the values of Fe_{1km} have been estimated for the time period from ~50 to ~6 Ma within the southern section (Fig. 5.12C) and for the time periods from ~130 to ~70 Ma BP and from ~15 to 0 Ma BP within the northern section in the Atlantic Ocean (Fig. 5.12D). The positions of these sections both to the east and to the west of the Mid-Atlantic Ridge axis were taken into account, and the values of Fe_{1km} have been calculated as half-sums of the values for the eastern and western flanks of the ridge when obtaining data and results for comparison.

On the average the values of Fe_{1km} for the sections in the Atlantic Ocean are 10 to 20 times lower than those for the sections in the Pacific Ocean. Obviously major differences are caused mainly by the much slower spreading rates of the Mid-Atlantic Ridge in comparison with the East Pacific Rise. Presumably the direction of the bottom currents in the section areas is another reason. In the Pacific Ocean the particulate hydrothermal matter has been transported mainly in a latitudinal direction and this has favored its accumulation on the flanks of the EPR. In the Atlantic Ocean the parti-

culate hydrothermal matter has been transported mainly in longitudinal directions (Lisitzin et al. 1980a). This would account for a reduction in the amount of particulate hydrothermal matter deposited on the flanks of the MAR in the sections sampled, and the morphology of the MAR could be another reason for the deposition of a reduced amount of hydrothermal matter. With low spreading rates, practically no hydrothermal matter leaves the rift valley and it does not reach the flank areas (Fig. 4.5). With an increase in the spreading rate, which could be up to threefold (see Fig. 5.13), not only hydrothermal activity and the incidence of hydrothermal plumes increased. The morphology of the rift probably also changed and particulate hydrothermal matter was released to the flanks of the ridge (Fig. 4.5). During the Cretaceous time, because of the lower vertical gradients of temperature and salinity in the ocean water, hydrothermal plumes could rise much higher above the ocean bottom than at present (Vogt 1989) and particulate hydrothermal matter also could leave the rift valley and reach the flank areas.

Section subparallel to the EPR axis between 5°S and 12°N. Reconstruction of the history of hydrothermal activity and mineral formation along the EPR axis between 5°S and 12°N in the last 18 Ma has been carried out on materials obtained during the study of sediment samples from the cores of the ODP Leg 138 (the collection of M. Levitan). Seven stations of this Leg have been located along a section that is more than 1600 km long on the western flank of the EPR and subparallel to the EPR axis (Fig. 5.16). The half-rate of spreading in this segment of the EPR is 6 to 8 cm a^{-1}.

Both metalliferous and non-metalliferous sediments with admixture of the hydrothermal metal-bearing matter were collected in these cores (Mayer et al. 1992; Gurvich et al. 1995b). The hydrothermal metal-bearing matter was contributed to these sediments from the axial part of the EPR. Chemical composition of the sediments at ODP Sites 845, 846, 848–854 and DSDP Site 83 has been studied by Gurvich et al. (1995b). Data for these sediments together with data for the sediment age and physical properties from Hays (1972), Mayer et al. (1992), and Shackleton et al. (1995), have been used for calculating the rates of accumulation of the hydrothermal Fe. The values of Fe_h* have been averaged for every 0.5 Ma period and plotted along the backtracked paths of the sites. For Sites 848 to 854 isopleths of the values of Fe_h* in spatiotemporal dissection have been drawn, and for Sites 845, 846, and 83 graphs of the values of Fe_h* along the backtracked paths have been drawn (Fig. 5.16).

It is clearly shown in Fig. 5.16 that maximum values of Fe_h* occur in the basal sediments that accumulated in the vicinity of the EPR axis. They are similar to the values that occur in the vicinity of the EPR axis within the recent field of metalliferous sediments in the Southeast Pacific (Fig.

1.24), and in basal metalliferous sediments collected during DSDP Legs 9, 16, and 85 (Fig. 5.10B; Leinen and Stakes 1979; Jarvis 1985), but lower than in recent and ancient metalliferous sediments that accumulated in the axial part of the EPR at 19°S to 22°S (Fig. 5.9A, 5.10A).

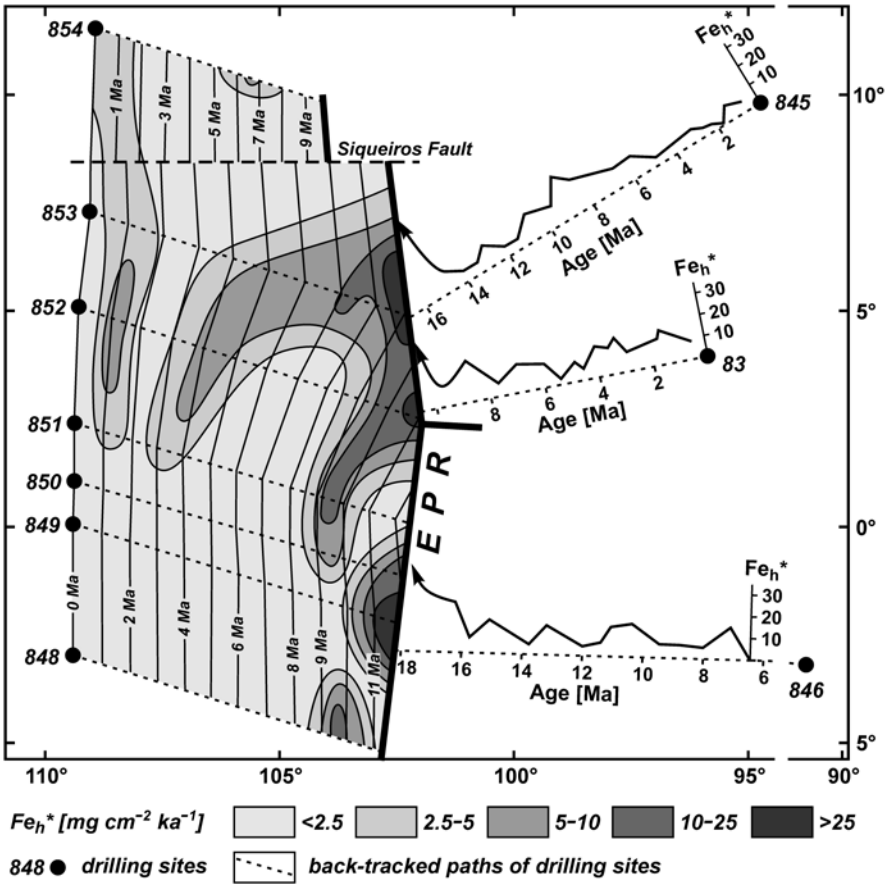

Fig. 5.16. Accumulation rates of hydrothermal Fe in bottom sediments of the section on the western flank of the EPR between 5°S and 12°N subparallel to the EPR axis in spatiotemporal dissection, and in bottom sediments along the backtracked paths of Sites 845, 83, and 846.

The isopleth plot demonstrates the temporal evolution of Fe_h* in surface sediments in a section subparallel to the EPR axis that gradually diverges from the axis along with the Pacific plate with the half-rate of spreading. The graphs showing data plotted for Sites 845, 846, and 83 demonstrate

temporal evolution of Fe_h* in surface sediments along the backtracked paths of these sites (Fig. 5.16).

The values of Fe_h* in the sediments from the eastern flank of the EPR are approximately twice as high as those in the sediments from the western flank located at the same latitude at similar distances from the EPR axis. Apparently this distribution of data is evidence, which shows that, at least since 12–10 Ma BP to the present time, the transport of the hydrothermal particulate matter in an easterly direction has prevailed in the area of the section between 5°S and 12°N. It is in good agreement with the results obtained in studies of the hydrology in the area, which show that at the present time the bottom water moves eastward mainly and across the EPR axis (Lonsdale 1976), and the results of paleooceanological studies show that in former times the eastward and northeastward movement of the bottom water in this area has prevailed at least since Eocene time (Lisitzin et al. 1980a). The diagram in Fig. 5.16 enables the characterization of the intensity and position of the hydrothermal activity along the EPR axis in the general features only, because the changes in the values of Fe_h* related to the increase in distance from the EPR axis were not considered, and the distance of the section from the axis is as great as 850 km.

In Sect. 4.7 it was shown that for distances from 20 to 2000 km from the EPR axis the average relationship of a decrease in the Fe_h* at the distance D (km) from the EPR axis, in comparison with that for Fe_h* at 20 km distance from the EPR axis, is clearly shown by the equation (4.3):

$$Fe_h^*/Fe_{h20}^* = (1.58–0.446\lg D)^2.$$

Based on the known values of Fe_h* in the sediments and the distances of the points of their deposition from the EPR axis it is possible to estimate the values of Fe_h* at different distances from the axis.

Estimates of this kind have been made for 11 temporal intervals from 12–10.5 Ma BP to 0.5–0 Ma BP, and diagrams showing reconstructions of the distribution of Fe_h* on the western flank of the EPR during these intervals have been drawn (Fig. 5.17). In these diagrams the near-axial values of Fe_h* correspond to a distance of 20 km from the EPR axis, the boundary value for the equation (4.3). Areas of intensive and very intensive hydrothermal activity and mineral formation on the EPR axis that occurred in the geological past are clearly visible on these diagrams. In sediments adjacent to these areas the reconstructed values of Fe_{h20}* are 10–25 and >25 mg cm^{-2} ka^{-1} respectively. They are the values determined for the western flank of the EPR oriented against the predominant direction of bottom currents. Actually the sediments of the section have accumulated on the western flank of the EPR and a correction for the bottom currents has not been made in the reconstructed values of Fe_h* at a distance of 20 km to the west of the EPR axis.

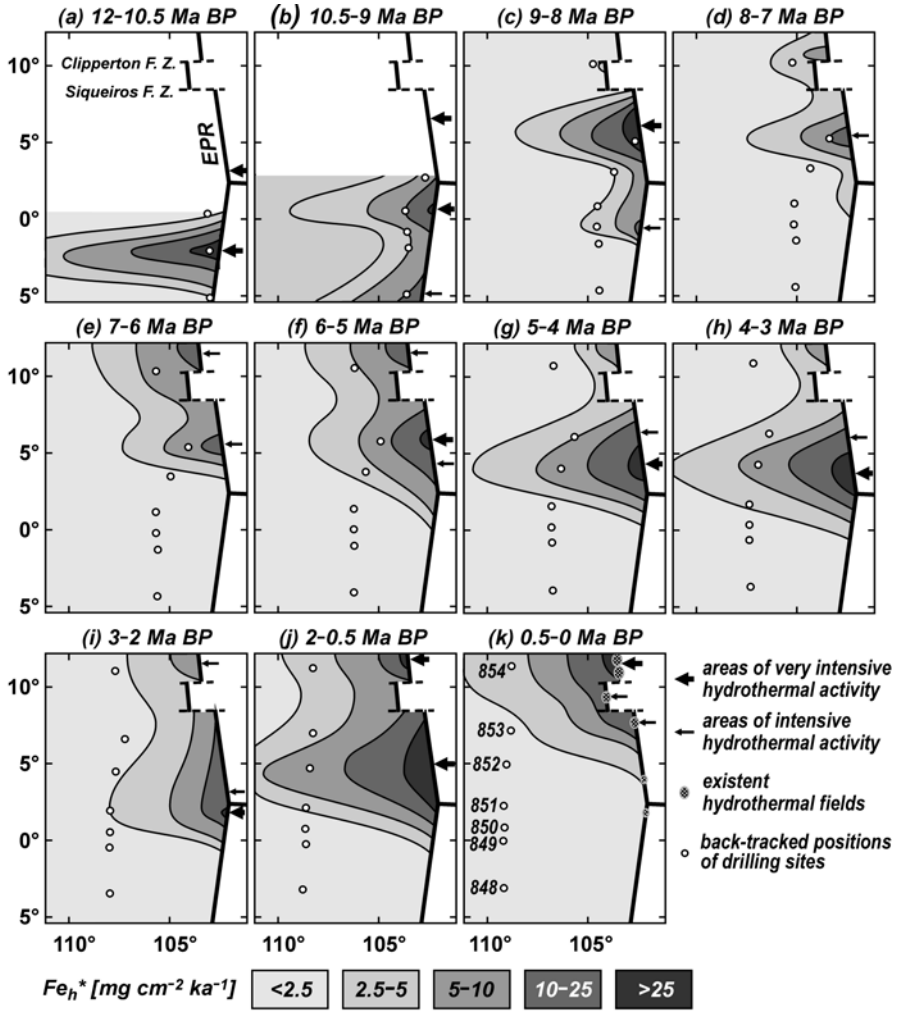

Fig. 5.17. Diagrams of paleodistribution of Fe_h* in bottom sediments to the west of the EPR axis and reconstructed positions and relative intensities of hydrothermal activity on the EPR axis for the last 12 Ma. The positions of the hydrothermal fields that existed are from Hekinian et al. (1983, 1985), Hekinian and Fouquet (1985), Gente et al. (1986), McConachy et al. (1986), Fouquet et al. (1988, 1996), Haymon et al. (1991), Poroshina et al. (1992), Baker et al. (1994), Von Damm (1995), Shank et al. (2000), Hannington et al. (2002).

12 to 10.5 Ma BP. Sediments accumulated during this time have been collected at Sites 848–850, 852, 845, 846, and 83 (Fig. 5.16). Low values of Fe_h* (<2.5 mg cm^{-2} ka^{-1}) in the basal sediments from Site 848, accumulated >11 Ma BP (Fig. 5.17a), are evidence of the absence of hydrothermal

activity in the vicinity of their deposition points. Later, 11–10 Ma BP, hydrothermal activity of low intensity may have developed in this area. High values of Fe_h*, up to 60 mg cm^{-2} ka^{-1}, occur in the near-axial sediments from Site 849 that accumulated 11.5 to 11 Ma BP. Apparently this is evidence of the existence of very intensive hydrothermal activity at this time on the EPR axis in the area of 2°–3°S (Fig. 5.17a). This activity existed during ~1.5 Ma. High values of Fe_h* (>25 mg cm^{-2} ka^{-1}) in the basal sediments from Site 83 and, probably, from Site 852 (there are no data for these sediments) (Fig. 5.16) are evidence that indicates that from ~11 to 10.5 Ma BP very intensive hydrothermal activity existed on the EPR axis in the area of ~3°N (Fig. 5.17a) and that about 10 Ma BP it decreased.

10.5 to 9 Ma BP. In sediments from Site 845 that accumulated at this time at a distance about 400 km from the EPR axis the values of Fe_h*, ~10 mg cm^{-2} ka^{-1}, are comparable to those for Fe_h* in sediments from Site 83 that accumulated approximately 40 to 50 km from the EPR axis (Fig. 5.16). Obviously this is evidence of the existence of very intensive hydrothermal activity ~10 Ma BP on the EPR axis that was located to the north of the point of accumulation of the sediments from Site 83, and presumably it was in the area between 5°S and 7°S. Increased values of Fe_h* occur in the non-basal sediments from Sites 848, 850, 851 that accumulated during this time period (Fig. 5.16). Apparently this is evidence of hydrothermal activity on the EPR axis in the areas 5°S and 1°N (Fig. 5.17b). According to the reconstructed values of Fe_{h20}*, at 5°–7°N and 1°N there was very intensive hydrothermal activity and it was less intensive at 5°S. About 9 Ma BP an increase occurred in the values of Fe_h* in the sediments in the southern and northern sections in the Pacific Ocean apparently as a result of an increase in the spreading rate (Fig. 5.12).

9 to 8 Ma BP the values of Fe_h* in the sediments from Sites 848–852 were relatively low, <5 mg cm^{-2} ka^{-1} or zero (Fig. 5.16). The reconstructed values of Fe_{h20}* (Fig. 5.17c) are evidence of hydrothermal activity of low intensity or its absence on the EPR axis in the southern part of the area in question. Only in the area 0° to 1°S near the axis of the EPR are the reconstructed values of Fe_{h20}* from 10 to 25 mg cm^{-2} ka^{-1} (Fig. 5.17c), and the reconstructed values of Fe_{h20}* in the sediments from Sites 845, 853, and 83 are evidence of the existence of hydrothermal activity in the central part of the area. Apparently the highest intensity was located between 5°N and 7°N (Fig. 5.17c). Hydrothermal activity was low in intensity or absent in the northern part of the area.

8 to 7 Ma BP the values of Fe_h* in the sediments from Sites 848 to 852 were low, <2.5 mg cm^{-2} ka^{-1} or zero (Fig. 5.16). The reconstructed values near the axis (Fig. 5.17d) are evidence of hydrothermal activity of low intensity or its absence on the EPR axis in the southern half of the area. In

the sediments from other sites and especially from Sites 853 and 845 the values of Fe_h* were much higher (Fig. 5.16). The reconstructed values of Fe_{h20}*, 10 to 25 mg cm^{-2} ka^{-1}, in the sediments to the west of the EPR (Fig. 5.17d) are evidence that 8 to 7 Ma BP intensive hydrothermal activity existed only in the area of 5°–6°N. At this time hydrothermal activity of low intensity probably appeared to the north of the Clipperton Fracture Zone.

7 to 6 Ma BP the pattern in general was similar. Hydrothermal activity persisted in the area of 5°–6°N. However, the increase in Fe_h* in the sediments from Site 854 (Fig. 5.16) is evidence that hydrothermal activity north of the Clipperton Fracture Zone increased at this time and the reconstructed values of Fe_{h20}* are 10 to 25 mg cm^{-2} ka^{-1} (Fig. 5.17e).

The increase in Fe_h* in the sediments from Site 846 accumulated ~8–6.5 Ma BP (Fig. 5.16), presumably, can be attributed to the deposition point of these sediments. They accumulated directly north of the ancient Galapagos Rise at the period of time from 8.2 to 6.5 Ma BP when both the EPR and the ancient Galapagos Rise were active (Mammerickx et al. 1980).

6 to 5 Ma BP the values of Fe_h* in the sediments from Sites 848 to 851 and 846 were low, <2.5 mg cm^{-2} ka^{-1} or zero. The value of Fe_h* in the sediments from Site 852 increased in spite of the increase in the distance from the place of their deposition to the EPR axis. In sediments from Site 853 the value of Fe_h* persisted (Fig. 5.16). The reconstructed value of Fe_{h20}* at ~5°–6°N exceeds 25 mg cm^{-2} ka^{-1} (Fig. 5.17f). This is evidence of very intensive hydrothermal activity on the EPR axis. Hydrothermal activity persisted to the north of the Clipperton Fracture Zone, however a decrease in the Fe_h* values in the sediments from Site 854 (Fig. 5.16) indicates that it became less intensive.

5 to 3 Ma BP the values of Fe_h* in the sediments from Sites 848 to 850, and 846 were low, <2,5 mg cm^{-2} ka^{-1} or zero. The increase in the Fe_h* values in the sediments from Site 852 persisted and reached a maximum, >5 mg cm^{-2} ka^{-1}, 5–4 Ma BP. About 4–3 Ma BP the value of Fe_h* in the sediments from Site 851 increased to 2.5–5 mg cm^{-2} ka^{-1}. The value of Fe_h* also increased in the sediments from Site 83 and was >10 mg cm^{-2} ka^{-1} in the time period from 4 to 3 Ma BP. In the sediments from Sites 853, 854, and 845 the values of Fe_h* gradually decreased (Fig. 5.16). The reconstructed values of Fe_{h20}* (Fig. 5.17g,h) indicate that in the southern part of the area in question from 5 to 3 Ma BP the hydrothermal activity on the EPR axis was low in intensity or absent. In the northern part of the area, from 2°–3°N to 5°–6°N, it was more intensive. Hydrothermal activity decreased to the north of the Clipperton Fracture Zone.

3 to 2 Ma BP the values of Fe_h* in the sediments of all of the sites, except for Sites 851 and 83, were very low or zero (Fig. 5.16). The reconstru-

cted values of Fe_{h20}* are evidence that at this time very intensive hydrothermal activity occurred in the area at ~2°N (Fig. 5.17i).

From 6–5 Ma BP to 3–2 Ma BP the area of very intensive hydrothermal activity moved along the EPR axis over a distance of 400–450 km (from 5°–6°N to ~2°N). The average rate of this movement was about 15 cm a^{-1}.

2 to 0.5 Ma BP the values of Fe_h* in the sediments from Sites 848 to 850, and 846 were very low or zero. In the sediments from Sites 851 to 853 accumulated ~700 km to the west of the EPR axis the values of Fe_h* increased to >2.5 mg cm^{-2} ka^{-1}. A maximum in the Fe_h* values was reached ~1 Ma BP. The value of Fe_h* also increased and exceeded 2.5 mg cm^{-2} ka^{-1} in the sediments from Site 854 in the time period from ~2–1.5 Ma BP to at least 0.3 Ma BP (when the youngest sediments studied from Site 854 accumulated). On the eastern flank of the EPR, in the sediments from Sites 845 and 83, the value of the Fe_h* increased, reached a maximum about 1.5 Ma BP, and then decreased (Fig. 5.16). Apparently the distribution of the reconstructed values of Fe_{h20}* (Fig. 5.17j) indicates the existence of very intensive hydrothermal activity between the Siqueiros Fracture Zone and the area of the Galapagos Triple Junction from 2 to 0.5 Ma BP, on the one hand, and on the other hand they may indicate the appearance of very intensive hydrothermal activity north of the Clipperton Fracture Zone. There are other data that are evidence of the latter. Basal metalliferous sediments that accumulated from 2.2 to 1.1 Ma BP were sampled in the vicinity of the Clipperton Fracture Zone during DSDP Leg 54 (Rosendahl et al. 1980). According to the estimations that were based on the results from this Leg (Rosendahl et al. 1980; Donnelly 1980a,b; Schrader et al. 1980), the values of Fe_h* in these sediments range from tens to hundreds of mg cm^{-2} ka^{-1}.

0.5 to 0 Ma BP the values of Fe_h* in the sediments from all the sites to the west of the EPR axis, except for Sites 854 and 853, were zero. In the sediments from Site 854 the value of Fe_h* exceeded 2.5 mg cm^{-2} ka^{-1} (Fig. 5.16), in the sediments from Site 853 it was about 2 mg cm^{-2} ka^{-1}. The distribution of the reconstructed values of Fe_{h20}* (Fig. 5.17k) is an evidence of the existence of very intensive hydrothermal activity north of 11°N, and of intensive hydrothermal activity between 11° and 7°N. Apparently the very intensive hydrothermal activity that existed from 2 to 0.5 Ma BP in the area between the Siqueiros Fracture Zone and the area of the Galapagos Triple Junction became extinct.

The reconstructed values of Fe_{h20}* between 11°N and 12°N, >25 mg cm^{-2} ka^{-1}, and between 7°N and 11°N, 10–25 mg cm^{-2} ka^{-1}, are close to the average values of Fe_h* in recent metalliferous sediments in the vicinity of the EPR axis in the area between 11°N and 14°N where the values, estimated from data of Lisitzin (1978) and Cherkashev (1990, 1992), range from 20 to 50 mg cm^{-2} ka^{-1}. Agreement in the data such as this encourages and

allows one to consider the diagrams in Fig. 5.17a-k as reasonably accurate, especially since the accuracy of the reconstructed values for the recent sediments, accumulated at the longest distance (~600 km) from the EPR axis, is the lowest.

The reconstructed locations of recent (0.5–0 Ma BP) areas of hydrothermal activity coincide with the positions of the existing hydrothermal fields along the EPR axis (Fig. 5.17k). At present hydrothermal activity of greatest intensity and associated mineral formation on the EPR axis within the area in question exists to the north of the Clipperton Fracture Zone between 11°N and 13°N; the areas of intensive hydrothermal activity and mineral formation occur between the Clipperton and Siqueiros Fracture Zones; the areas with hydrothermal activity of lower intensity and mineral formation are at ~7°N, ~4°N, and ~2°N (Fig. 5.17k). If the reconstruction for the time period from 2 to 0.5 Ma BP is correct, it is evident that very intensive hydrothermal activity developed at this time on the EPR axis between 11°N and 13°N.

During the last 12 Ma massive accumulations of hydrothermal sulfide minerals formed in the hydrothermal fields along the EPR between 5°S and 12°N. The approximate place and time of their formation can be determined from the locations of the reconstructed areas of hydrothermal activity (Fig. 5.17a-k). Because of the movement of the Pacific lithosphere plate at the present time these accumulations or their remnants are located at different distances from the EPR axis. If these accumulations have been preserved and covered by sediments or lava flows, their present locations apparently coincide with the areas that have high accumulation rates of hydrothermal Fe in the lowermost basal sediments. The locations of these sediments and the accumulation rates of hydrothermal Fe on the EPR axis, reduced to the distance of 2.5 m from hydrothermal vents ($Fe_h*_{2.5}$), can be estimated from the data for the sediments from the drilling cores of the section explored to the west of the EPR axis (Fig. 5.16). In this reconstruction as well as in the reconstructions based on the studies of sediment cores (Sect. 5.1) it is assumed that: a) the hydrothermal Fe has been contributed to the sediments only from hydrothermal plumes or their fragments; and b) the accumulation rate of the hydrothermal Fe at the time of deposition of the sediments was equal to its settling flux. Estimations have been made by using a combination of the two equations (4.1) and (4.3) and with the application of corrections for bottom currents. The complex graph used in obtaining the reconstructed values of $Fe_h*_{2.5}$ from the values of Fe_h* and the distance from the EPR axis is shown in Fig. 5.14. In the case of the sediments from the western flank of the EPR and the predominant easterly direction of the bottom currents the line "for a flank oriented against a predominant bottom current direction" can be used. The difference between figures on this line and the line "for a

flank oriented to a predominant bottom current direction"[42] is a factor of ~0.5, which has been estimated by comparing the values for Fe_h* in sediments from the eastern and western flanks of the EPR that accumulated at the same latitude and at similar distances from the EPR axis.

The calculated reconstructed values of $Fe_h*_{2.5}$ have been plotted along the backtracked paths of the drilling sites with reference to the age of the sediments from the lowermost part of the basal layer or the age of the crust (Fig. 5.18B). The range of variations of the values of $Fe_h*_{2.5}$ on the EPR axis between 5°S and 12°N during the last 12 Ma is from <1000 to 7500 mg cm^{-2} ka^{-1}. The values of $Fe_h*_{2.5}$ corresponding to the more intensive, >4000 mg cm^{-2} ka^{-1}, and less intensive, 2000–4000 mg cm^{-2} ka^{-1}, hydrothermal activity are approximately twice as low as that on the EPR axis between 20°30'S and 22°00'S during the last 50 ka (Fig. 5.9). This is in good agreement with the general relationship of the accumulation rate of the hydrothermal Fe with the spreading rate, other factors being consistent. Between 5°S and 12°N the half-rate of spreading is 6 to 8 cm a^{-1}, and between 20°30'S and 22°00'S it is ~10 cm a^{-1}. According to the general relationships shown in Figure 4.35, when the half-rate of spreading is 6 to 8 cm a^{-1}, the Fe_h* value is approximately twice as low as it is when the spreading rate is 10 cm a^{-1}.

High settling fluxes and accumulation rates of the hydrothermal Fe in sediments near hydrothermal vents usually accompany the formation and accumulation of sulfide minerals within hydrothermal fields. That is why Fig. 5.18B shows not only the reconstructed distribution of the near-vent accumulation rates of the hydrothermal Fe and the values of Fe_h* in the lowermost part of the basal sediment layer, but also the recent locations of the areas where there are buried accumulations of hydrothermal sulfide minerals (if they have been preserved) that formed during the last 12 Ma along the EPR axis and moved to the west-northwest with the Pacific plate. The higher the values of Fe_h* in the lowermost part of the basal sediment layer the greater the probability of occurrence of buried accumulations of hydrothermal sulfide minerals. Obviously the quantitative aspects of this relationship will be defined in the future.

It must be noted that apparently huge masses of hydrothermal polymetallic mineral matter that formed during the last ~150 Ma are buried in the present ocean. This matter is rich in Fe, Cu, Zn, and other metals. Estimates for the accumulation of the hydrothermal polymetallic mineral matter formed on the axis of the East Pacific Rise and buried at present in

[42] This line can be used for the sediments from the section located to the west of the EPR axis between 20°30'S and 22°00'S (Fig. 5.9) where the westerly direction of the bottom currents prevails.

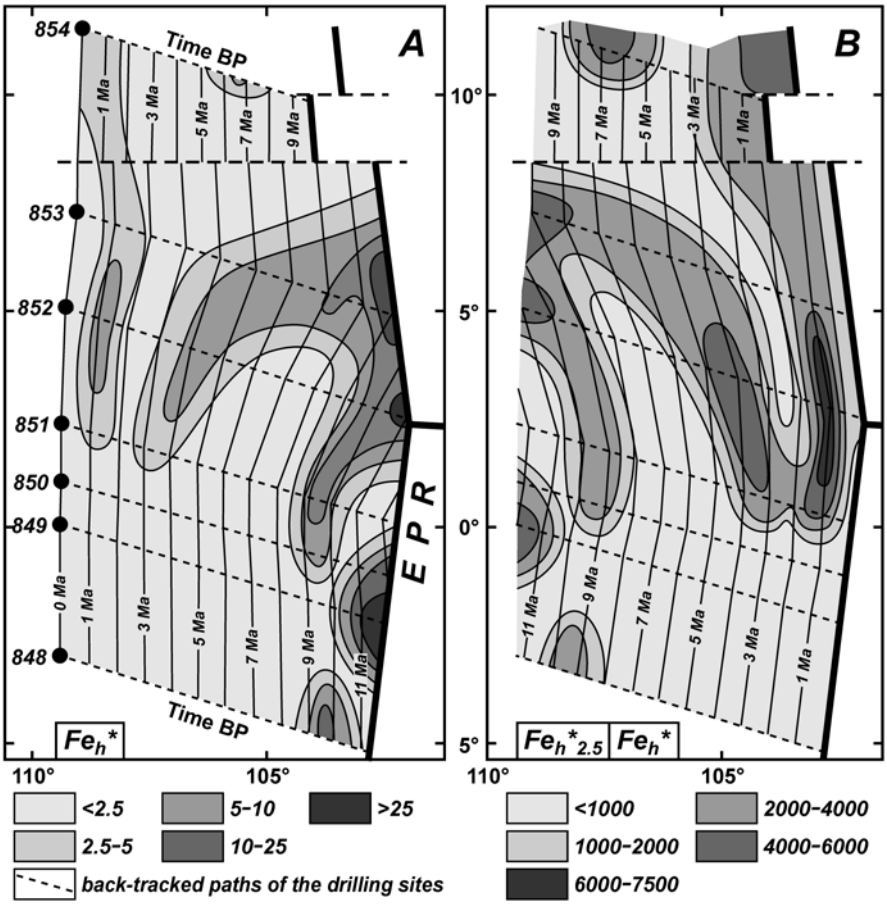

Fig. 5.18. A – Temporal evolution of Fe_h* [mg cm^{-2} ka^{-1}] in surface sediments in the last 12 Ma along a section subparallel to the EPR axis and gradually moving to the west-northwest from the axis with the half-rate of spreading. B – Reconstruction of $Fe_h*_{2.5}$ [mg cm^{-2} ka^{-1}] for the last 12 Ma as well as the distribution of Fe_h* [mg cm^{-2} ka^{-1}] in the lowermost sediments of the basal sediment layer within the area from the section to the EPR axis. Isochrones show sediment and crust age. The distribution reflects the probability of present occurrence of buried accumulations of hydrothermal sulfide minerals.

the Pacific can be made for the benefit of discussion and argument. In the metalliferous sediments in the Southeast Pacific $550 \cdot 10^3$ tons of hydrothermal Fe accumulates annually (Table 1.2). If this amount is considered to be dispersed hydrothermal Fe (actually the amount is greater because not all of the dispersed hydrothermal Fe accumulates in the metalliferous sediments), but it comprises 95–98% of the total hydrothermal contribution of

Fe, which is estimated $(560 \div 580) \cdot 10^3$ t a^{-1}. 2–5% of this amount, that is $(10 \div 30) \cdot 10^3$ t a^{-1}, accumulates in the massive hydrothermal metallic mineral material. If this is considered to be an average amount, during $150 \cdot 10^6$ years along the East Pacific Rise $(1.5 \div 4.5) \cdot 10^{12}$ tons of the Fe accumulated in the massive hydrothermal metallic mineral matter. If the average content of Fe in this matter is ~30%, then an amount of the massive hydrothermal metallic mineral matter for recovery and use is ca. $(5 \div 15) \cdot 10^{12}$ tons. This matter (if it is preserved) is covered by sediments or lava flows and it is located in the Pacific Ocean to the west-northwest and to the east of the East Pacific Rise axis.

5.3. Scale and dimension of reconstructions

In previous sections of this book it has been shown that metalliferous and low-metalliferous sediments provide information that can be used in the reconstruction of the history of hydrothermal activity and in the search for accumulated and buried hydrothermal mineral deposits of significant economic value as mineral resources. The data and concepts from the research on the proximal and distal metalliferous sediments reported here can be used for different kinds of reconstruction of the history of these deposits and can provide essential data for locating and evaluating them as mineral resources.

The studies of the proximal metalliferous sediments enable the reconstruction of the history of hydrothermal activity and mineral formation within individual hydrothermal fields and the search of large hydrothermal mineral accumulations and answer questions related to their position and composition when exploring and evaluating them as resources. The parameters that can be reconstructed and that have been considered are shown in Table 5.1.

The properties of the proximal metalliferous sediments that accumulated within hydrothermal fields of fast, medium, and slow-spreading rifts are similar. But the occurrence and intensity of high-temperature hydrothermal activity on slow-spreading ridges is much lower than on medium- and fast-spreading ridges. High-temperature hydrothermal fields are far apart on the slow-spreading ridges (German and Parson 1998), and fields of distal metalliferous sediments are small or absent. If they do form they usually occur within deep rift valleys, because the nonbuoyant hydrothermal plumes rarely extend beyond such valleys (Sect. 4.3). Fields of distal metalliferous sediments of considerable size can form in the vicinity of groups or numerous groups of hydrothermal fields, and only their combined contribution

Table 5.1. Scales of reconstruction of the history of hydrothermal activity and mineral formation and of search for hydrothermal accumulations in the deep ocean by using materials from studies of metalliferous and low-metalliferous sediments.

Scales of studies / *studied sediments*	Spreading rates	Objects of reconstruction and search	Dimensions of objects, km	Distances to objects, km	Reconstructed and searched parameters of objects	Temporal intervals of reconstruction
Local / *proximal*	slow ÷ medium	large hydrothermal accumulations (active and relict) within hydrothermal fields	$n \cdot 10^{-1}$	$n \cdot 10^{-2} \div (1 \div 2)$	position of large hydrothermal accumulations, intensity of hydrothermal activity and mineral formation on them, metallogenic specialization	$0 \div n \cdot 10^{1}$ ka BP
Areal / *distal*	medium ÷ fast	hydrothermal fields (active and relict) and/or their groups, areas of occurrence of hydrothermal accumulations	$n \cdot 10^{0} \div n \cdot 10^{1}$	$n \cdot 10^{0} \div n \cdot 10^{1}$	position of hydrothermal fields and/or their groups, intensity of hydrothermal activity and mineral formation, present position of areas and probability of occurrence of hydrothermal accumulations	$0 \div n \cdot 10^{2}$ ka BP
Regional / *distal*	medium ÷ fast	areas of hydrothermal activity and mineral formation (recent and ancient) within large rift segments, areas of occurrence of hydrothermal accumulations	$n \cdot 10^{1} \div n \cdot 10^{2}$	$n \cdot 10^{1} \div n \cdot 10^{2}$	position of areas of recent and ancient hydrothermal activity and mineral formation, present position of areas and probability of occurrence of hydrothermal accumulations	$0 \div n \cdot 10^{1}$ Ma BP
Global / *distal*	slow ÷ fast	oceans and their parts	$>n \cdot 10^{3}$		intensity of hydrothermal activity and mineral formation	$0 \div 1.5 \cdot 10^{2}$ Ma BP

of hydrothermal matter can provide sufficient amounts of material for the formation of these sediments. For this reason fields of distal metalliferous sediments of considerable size can form only in and near medium-spreading and mainly fast-spreading ridges. The existence of such fields is evidence of the medium and fast spreading rates of ridges that are or were contributors of the metal-bearing matter to these sediments. It was shown in Sects. 5.1 and 5.2 how the results of studies of the distal metalliferous sediments enable the solving of problems in the reconstruction of their history, in the search and exploration for them and in determining their area and regional distribution. The parameters that can be reconstructed are shown in Table 5.1.

The manner of investigation and approach in the exploration and research of sections parallel or subparallel to the axes of spreading ridges can vary depending on the direction and velocities of bottom currents. The best areas for locating sections for investigation are those where the bottom currents are slow and their predominant directions of flow are across the spreading axes. The section to the west of the EPR axis from 5°S to 12°N is a good example (Fig. 5.16–5.18), where it has been shown that the distance of the sections from the axes of the spreading ridges can be hundreds of kilometers. Sections of minimum distance from the axes must enable the collection of cores that are of sufficient length for the studies. It is not necessary to use continuous core sections for the study and reconstruction of the sequence of historical events. Fragments of core sections can be used for obtaining information and data that are needed: the age of the sediments, the accumulation rate of the hydrothermal Fe, and the distance from the axis of the spreading ridge that contributed the hydrothermal matter to these sediments. However, in such cases the accuracy of the reconstructed history is reduced. In general, the closer the sediment strata studied are to the basement rocks the greater the accuracy. The equations 4.1 and 4.3, which have been used for the reconstructions, are not universal, and they describe the average relationships in the present Pacific and recent Southeast Pacific Ocean. In other areas and at other times in the geological history the character of such relationships could have been different. Corrections can be obtained from materials located at sections or strip-sections along spreading tracks or perpendicular to the axes of spreading ridges, especially if they are located on both flanks of ridges. They can give information on variations in the accumulation rates of the hydrothermal Fe with increasing distances from the axes of spreading ridges both at present and in the geological past.

It has been shown above that at the present time there are approaches and methods for the study of the geology of metalliferous sediments, and for the features or parameters that provide valuable information on the intensity of hydrothermal activity that produced mineral formation, on their

locations during geologic time, on the present position of areas and sites where buried hydrothermal accumulations of sulfide minerals can occur, and, in the case of proximal metalliferous sediments, on the locations and special metallogenic features of the accumulations of hydrothermal sulfide minerals that are formed simultaneously with these sediments.

Undoubtedly, with further development of research methods the opportunities for exploration and the possibilities of reconstructing the history and genesis more specifically will be extended greatly in breadth and in accuracy. Nevertheless, the data available at the present time, obtained in the study of the metalliferous sediments, enable the solving of exploration and research questions and the reconstruction of geological events on a local and regional scale. A list of the geological features and parameters considered today in research and in the reconstruction of geological events, the dimensions of features in different scales of studies and distances to them, as well as intervals of time for different scales of studies, are shown in Table 5.1.

Some notice is given in Table 5.1 to studies of a global scale. These can provide new and very important perspectives in the study of hydrothermal activity and mineral formation that have not as yet been considered.

There exists a number of approaches to the study of the global history of hydrothermal activity in the ocean. It is considered important to know the global evolution of hydrothermal mineral formation, climate of the Earth, composition of ocean water, etc. In approaches of this kind the evolution in the contents and ratios of chemical elements and/or their isotopes, which are proxies indicating the hydrothermal contribution to the ocean, are studied. But most of these elements have residence times that exceed the mixing time of the ocean water and cannot characterize particular oceans, let alone any of their parts. Iron, which is used as the main proxy for the content of hydrothermal material in metalliferous sediments, is of special and critical interest. According to my estimates, the hydrothermal contribution of Fe to the Pacific Ocean is about 40–50% of the total contribution of the labile Fe (the dissolved plus that precipitated from solution) to the deep ocean, and its residence time here is estimated about 10 years. From a geological point of view, the response of ocean sediments, and most of all the metalliferous sediments, to variations in the contributions of the hydrothermal Fe is practically instantaneous.

The physical-historical approach to studies of the accumulation of both the proximal and distal metalliferous sediments, as well as knowledge of the factors, which determine variations in the composition and accumulation rates of the metalliferous sediments, enable the reconstruction of the history of the hydrothermal activity and mineral formation within hydrothermal fields and within particular segments of the spreading ridges. In the

latter case the present positions of buried massive hydrothermal accumulations can be determined with some probability. This has important significance, especially for the East Pacific Rise, a part of the World Ocean rift system where the most intensive hydrothermal activity and mineral forming processes take place. On the EPR, at least during the last 150 million years, from 5 to 15 trillion (!) tons of polymetallic hydrothermal metal-bearing material have formed. This material has been covered by sediments and lava flows and is located in the Pacific Ocean to the east and to the west-northwest of the EPR axis. At the present time this enormous mineral resource that is rich in such elements as Fe, Cu, Zn, etc. is not recoverable. However, as engineering and technological methods are developed, specific attention will be paid to this obvious and enormous source of metals and minerals. Research and the results of studies of the metalliferous sediments will provide essential information for use in the prospecting and exploration for them.